

TKK Dissertations 139
Espoo 2008

**CHARACTERIZATION OF DIFFUSERS
AND LIGHT-EMITTING DIODES USING
RADIOMETRIC MEASUREMENTS AND
MATHEMATICAL MODELING**

Doctoral Dissertation

Pasi Manninen



**Helsinki University of Technology
Faculty of Electronics, Communications and Automation
Department of Signal Processing and Acoustics**

TKK Dissertations 139
Espoo 2008

**CHARACTERIZATION OF DIFFUSERS
AND LIGHT-EMITTING DIODES USING
RADIOMETRIC MEASUREMENTS AND
MATHEMATICAL MODELING**

Doctoral Dissertation

Pasi Manninen

Dissertation for the degree of Doctor of Science in Technology to be presented with due permission of the Faculty of Electronics, Communications and Automation for public examination and debate in Auditorium S4 at Helsinki University of Technology (Espoo, Finland) on the 21st of November, 2008, at 12 noon.

**Helsinki University of Technology
Faculty of Electronics, Communications and Automation
Department of Signal Processing and Acoustics**

**Teknillinen korkeakoulu
Elektroniikan, tietoliikenteen ja automaation tiedekunta
Signaalinkäsittelyn ja akustiikan laitos**

Distribution:

Helsinki University of Technology
Faculty of Electronics, Communications and Automation
Department of Signal Processing and Acoustics
Metrology Research Institute
P.O. Box 3000
FI - 02015 TKK
FINLAND
URL: <http://spa.tkk.fi/>
URL: <http://metrology.tkk.fi/>
Tel. +358-9-4511
Fax +358-9-451 2222
E-mail: pasi.manninen@tkk.fi

© 2008 Pasi Manninen

ISBN 978-951-22-9555-5
ISBN 978-951-22-9556-2 (PDF)
ISSN 1795-2239
ISSN 1795-4584 (PDF)
URL: <http://lib.tkk.fi/Diss/2008/isbn9789512295562/>

TKK-DISS-2508

Picaset Oy
Helsinki 2008



ABSTRACT OF DOCTORAL DISSERTATION		HELSINKI UNIVERSITY OF TECHNOLOGY P.O. BOX 1000, FI-02015 TKK http://www.tkk.fi	
Author Pasi Urpo Matias Manninen			
Name of the dissertation Characterization of Diffusers and Light-Emitting Diodes Using Radiometric Measurements and Mathematical Modeling			
Manuscript submitted 2 nd June 2008		Manuscript revised 25 th September 2008	
Date of the defence 21 st November 2008			
<input type="checkbox"/> Monograph		<input checked="" type="checkbox"/> Article dissertation (summary + original articles)	
Faculty Faculty of Electronics, Communications and Automation			
Department Department of Signal Processing and Acoustics			
Field of research Measurement Science and Technology			
Opponent(s) Dr. Peter Blattner, Federal Office of Metrology (METAS), Switzerland			
Supervisor Prof. Erkki Ikonen			
Instructor Doc. Petri Kärhä			
Abstract <p>Entrance diffusers enable good cosinusoidal angular responsivities of optical detectors. However, they also affect the position of the apparent detector receiving plane (reference plane). In this thesis, the reference planes of four spectroradiometer diffusers have been investigated and found to be located, in most cases, inside the diffuser. The reference plane shift should be taken into account in the calibration of the spectroradiometer equipped with such a diffuser. If the reference plane shifts are omitted, the measurement results may become systematically erroneous. The reference plane distance offsets correlate with their angular responsivities. Thus, with available angular responsivity data of a diffuser, the need to measure accurately the reference plane offset of the diffuser can be evaluated. The results obtained can be utilized in solar ultraviolet irradiance measurements.</p> <p>In the thesis, new kinds of measurement methods for characterizing photometric properties of light-emitting diodes (LEDs) have also been developed. The modified inverse-square law method has been developed for analyzing LED illuminance at varying distances. The method has been tested for several LEDs with different packages, colors and power levels. The method gives information about the LED luminous intensity, the LED directivity and the size and location of the LED virtual image source. The new method developed is useful in designing LED-based luminaires when photometric characteristics of LEDs become more reliably predicted.</p> <p>Pulse-width modulation (PWM) is often used to dim LEDs. An LED is driven at pulsed current and by changing the duty cycle of the current the LED brightness can be controlled. The influence of the PWM on spectral, thermal, and colorimetric properties of low-power, epoxy-encapsulated LEDs have also been investigated. In the thesis, a measurement system, with which the LED temperature at different duty cycles could be determined, was constructed. Using the experimental set-up, the peak-wavelengths and bandwidths of LEDs under the PWM control were evaluated. A blueshift of the peak wavelength and bandwidth narrowing of the LEDs were found. The changes in the emission spectra of the LEDs were concluded to be caused by the changes in the LED temperature. Apparent color shifts, which can be perceived by the human eye, were observed in emitted colors of two LEDs. The results indicate that it would be useful to include information on optical and thermal properties of pulsed LEDs more in detail in the datasheets by the LED manufacturers.</p>			
Keywords Irradiance, solar ultraviolet, diffuser, light-emitting diode, luminous intensity, pulse-width modulation			
ISBN (printed) 978-951-22-9555-5		ISSN (printed) 1795-2239	
ISBN (pdf) 978-951-22-9556-2		ISSN (pdf) 1795-4584	
Language English		Number of pages 55 p. + app. 34 p.	
Publisher Helsinki University of Technology, Metrology Research Institute			
Print distribution Helsinki University of Technology, Metrology Research Institute			
<input checked="" type="checkbox"/> The dissertation can be read at http://lib.tkk.fi/Diss/2008/isbn9789512295562/			



VÄITÖSKIRJAN TIIVISTELMÄ	TEKNILLINEN KORKEAKOULU PL 1000, 02015 TKK http://www.tkk.fi
Tekijä Pasi Urpo Matias Manninen	
Väitöskirjan nimi Diffuuserien ja loistedioidien karakterisointi hyödyntämällä radiometrisia mittauksia ja matemaattista mallinnusta	
Käsi kirjoituksen päivämäärä 2.6.2008	Korjatun käsi kirjoituksen päivämäärä 25.9.2008
Väitöstilaisuuden ajankohta 21.11.2008	
<input type="checkbox"/> Monografia	<input checked="" type="checkbox"/> Yhdistelmäväitöskirja (yhteenvedo + erillisartikkelit)
Tiedekunta	Elektroniikan, tietoliikenteen ja automaation tiedekunta
Laitos	Signaalinkäsittelyn ja akustiikan laitos
Tutkimusala	Mittaustekniikka
Vastaväittäjä(t)	Toht. Peter Blattner, Federal Office of Metrology (METAS), Sveitsi
Työn valvoja	Prof. Erkki Ikonen
Työn ohjaaja	Dos. Petri Kärhä
Tiivistelmä Työssä kehitettiin menetelmä spektrometrioiden diffuuserien referenssitason paikan määrittämiseksi. Diffuuserit mahdollistavat hyvän kosinivasteen irradianssia mittaavalle detektorille, mutta työssä havaittiin niiden vaikuttavan myös säteilyn vastaanottotason sijaintiin. Tulokset osoittivat, että referenssitaso sijaitsi usein diffuuserin sisällä vastoin aiempia oletuksia. Mikäli tätä ilmiötä ei oteta huomioon spektrometrioiden kalibroinnissa, tuloksena voi olla systemaattisesti virheellisiä mittauksia. Lisäksi havaittiin, että diffuuserien kosinivirheet korreloivat voimakkaasti niiden referenssitason siirtymien kanssa. Täten diffuuserin referenssitason siirtymän mittaustarvetta voitiin arvioida tunnetuista kosinivirheistä. Saavutettuja tuloksia voidaan hyödyntää esimerkiksi auringon ultraviolettisäteilyn mittausten kehittämisessä. Työssä kehitettiin lisäksi mittausmenetelmiä loistedioidien (light-emitting diode) fotometrinen ominaisuuksien karakterisoimiseksi. Loistedioidin valaistusvoimakkuuden etäisyysriippuvuuden mallintamiseksi johdettiin modifioitu käänteinen neliölaki. Tämän mallin rinnalle kehitettiin analyysimenetelmä, joka perustui loistedioidin suuntaavuuden ja valaistusvoimakkuuden tuntemiseen eri etäisyyksillä. Menetelmällä voitiin määrittää hyvin tarkasti loistedioidin valovoima sekä virtuaalisen kuvälähteen koko ja sijainti. Kehitetty menetelmä on hyödyllinen esimerkiksi loistedioidivalaisimien suunnittelussa, kun loistedioidien fotometrinen käyttäytyminen voidaan paremmin ennustaa. Pulssileveysmodulaatiota käytetään usein loistedioidien himmenysmenetelmänä. Loistedioidia ajetaan katkoviiralla ja viiran päälläolon suhteellista aikaa muuttamalla saadaan kirkkautta säädettyä. Tässä työssä tutkittiin pulssileveysmodulaation vaikutusta loistedioidien aallonpituusspektriin ja väriin. Lisäksi määritettiin loistedioidin liitoslämpötila eri käyttöasoilla. Loistedioidien aallonpituudet lyhenivät, kun loistedioidia himmennettiin. Muutokset loistedioidien spektreissä havaittiin lämpötilan muutosilmiöksi. Kahdelle loistedioidille löydettiin ihmissilmällä havaittavia värimuutoksia. Työn tulokset indikoivat, että loistedioidivalmistajien tulisi spesifioida tarkemmin loistedioidien spektraali- ja lämpöominaisuudet pulssituksen aikana.	
Asiasanat Irradianssi, auringon ultraviolettisäteily, diffuuseri, loistedioidi, valovoima, pulssileveysmodulaatio	
ISBN (painettu) 978-951-22-9555-5	ISSN (painettu) 1795-2239
ISBN (pdf) 978-951-22-9556-2	ISSN (pdf) 1795-4584
Kieli Englanti	Sivumäärä 55 s. + liit. 34 s.
Julkaisija Teknillinen korkeakoulu, MIKES TKK Mittaustekniikka	
Painetun väitöskirjan jakelu Teknillinen korkeakoulu, MIKES TKK Mittaustekniikka	
<input checked="" type="checkbox"/> Luettavissa verkossa osoitteessa http://lib.tkk.fi/Diss/2008/isbn9789512295562/	

PREFACE

The research work of this thesis has been carried out at the Metrology Research Institute (MRI) of Helsinki University of Technology during 2005 – 2008. I want to thank Professors Pekka Wallin and Erkki Ikonen for providing me the opportunity to work in the interesting field of optical metrology. Prof. Ikonen has given very valuable guidance and encouraged me during the work.

As well, I want to thank my instructor, Docent Petri Kärhä for giving helpful advices and useful discussions throughout this study, D.Sc. Jari Hovila for guiding me in the experimental part of my work in the field of radiometry and D.Sc. Pasi Orreveteläinen for rich discussions in the research fields of colorimetry and LEDs. I also express my gratitude to all the co-authors and colleagues at the MRI.

I wish to thank the preliminary examiners, Academy Professor Jari Turunen and Dr. Jarle Gran, for their efforts.

I acknowledge grants from the Jenny and Antti Wihuri Foundation, the Finnish Cultural Foundation, and the Research Foundation of Helsinki University of Technology.

Finally but not for the most minor, I thank my wife Joveini for her patience and important encouraging and my children Tuovi and Touko for the happy receptions when returning home after the hard working days.

Espoo, September 2008

Pasi Manninen

CONTENTS

LIST OF PUBLICATIONS.....	9
AUTHOR'S CONTRIBUTION.....	10
1 INTRODUCTION.....	11
1.1 MOTIVATION	11
1.2 SCOPE AND CONTENTS OF THE THESIS	13
1.3 CONTRIBUTION OF THE RESEARCH	14
2 MODELING ENERGY TRANSFER BETWEEN PARALLEL PLATES.....	16
2.1 MODEL EQUATIONS FOR INCANDESCENT LAMPS	16
2.1.1 <i>Comprehensive equation</i>	16
2.1.2 <i>Simplified equations</i>	21
2.2 MODEL EQUATIONS FOR DIODE EMITTERS.....	21
3 MODELING STANDARD LAMPS	24
3.1 DIRECTIVITY PARAMETERS.....	25
3.2 RADIANCE DISTRIBUTION AND OFF-CENTRICITY	25
3.3 ACCURACY OF THE LUMINOUS INTENSITY ANALYSIS.....	26
4 OPTICAL CHARACTERIZATION OF DIFFUSERS	28
4.1 ANGULAR RESPONSIVITIES.....	29
4.2 SPATIAL RESPONSIVITIES	30
4.3 RECEIVING PLANE POSITIONS.....	31
4.3.1 <i>Reference plane displacements and their significance</i>	32
4.3.2 <i>Evaluation of measurement need</i>	33
4.3.3 <i>Simplification of the analysis model</i>	34
5 ANALYZING INTENSITY OF DIODE EMITTERS	36
5.1 PRINCIPLE OF THE ANALYSIS METHOD	37
5.2 RESULTS OF THE LUMINOUS INTENSITY ANALYSES OF LEDs	37
5.3 SIMPLIFICATION OF THE METHOD	39
5.4 APPLICATIONS	40
6 BEHAVIOR OF LIGHT-EMITTING DIODES UNDER PULSE-WIDTH MODULATION	42
6.1 PULSE-WIDTH MODULATION SCHEME.....	43
6.2 EXPERIMENTAL SET-UP.....	43
6.3 RESULTS AND DISCUSSIONS	44
6.3.1 <i>Spectral power distributions</i>	44
6.3.2 <i>Junction temperatures</i>	45
6.3.3 <i>Color coordinates</i>	46
7 CONCLUSIONS.....	48
REFERENCES.....	50

LIST OF PUBLICATIONS

This thesis consists of an overview and of the following publications.

- P1. P. Manninen, J. Hovila, L. Seppälä, P. Kärhä, L. Ylianttila, and E. Ikonen, "Determination of distance offsets of diffusers for accurate radiometric measurements," *Metrologia* **43**, S120–S124 (2006).
- P2. P. Manninen, P. Kärhä, and E. Ikonen, "Determining the irradiance signal from an asymmetric source with directional detectors: application to calibrations of radiometers with diffusers," *Appl. Opt.* **47**, 4714–4722 (2008).
- P3. P. Manninen, J. Hovila, P. Kärhä, and E. Ikonen, "Method for analysing luminous intensity of light-emitting diodes," *Meas. Sci. Technol.* **18**, 223–229 (2007).
- P4. E. Ikonen, P. Manninen, and P. Kärhä, "Modeling distance dependence of LED illuminance," *Light & Engineering* **15**, 57–61 (2007).
- P5. P. Manninen and P. Orreveteläinen, "On spectral and thermal behaviors of AlGaInP light-emitting diodes under pulse-width modulation," *Appl. Phys. Lett.* **91**, 181121 (2007).

AUTHOR'S CONTRIBUTION

All the publications included in this thesis are results of team work of the authors.

For publications P1 and P2, the author of this thesis has conducted all the measurements, performed the data analyses, and prepared the manuscripts. The author derived the model equations for publication P2.

For publications P3 and P4, the author constructed the control electronics for LEDs and carried out all the measurements and data analyses. The author prepared the manuscript for publication P3.

For publication P5, the author developed the main idea, designed the pulse current source for LEDs, carried out all the measurements and most of the data analysis, and prepared the manuscript.

1 INTRODUCTION

1.1 MOTIVATION

The measurement activities of solar ultraviolet (UV) irradiance have recently increased quite a lot due to the role of the solar UV in monitoring changes in the ozone layer and harmful effects of the UV radiation. This has led to notable reductions in measurement uncertainties. In different parts of Europe, several monitoring measurement sites for solar spectral irradiance have been established to determine the solar UV radiation level on ground by using high-accuracy spectroradiometers [1-9]. These solar UV spectroradiometers have been equipped with high-quality, well-characterized, cosine-matched measuring heads or diffusers [10-12]. For calibrating the spectroradiometer in situ, handy field calibrator units have been developed [13-15].

Several studies have been made to determine optical properties of entrance diffusers [16-19]. However, choosing the appropriate reference plane for the calibration of the spectroradiometer has received relatively little attention. Usually, solar UV spectroradiometers are calibrated at distances of 500 mm or 700 mm from the spectral irradiance standard lamp. The calibration distances are measured from the outermost surface of the diffuser, because it is assumed to work as the reference plane of the spectroradiometer [20]. However, it is only an assumption that the inverse-square law works relative to that plane. Especially, it is obvious that the real receiving plane of dome-shaped diffusers, often used as measuring heads of solar UV spectroradiometers, is located inside the diffuser. Also, the reference planes may be influenced by the refraction properties of the diffusing material which can be a function of wavelength. The optical reference plane displacements for photometer diffusers have been found to be several millimeters [21]. It is of interest to investigate whether spectroradiometer diffusers have similar shifts, because, e.g., a displacement of 5 mm in a 500-mm measurement distance would produce an error of 2 % in the measurement results of the solar UV.

The inverse-square law is problematic also in the measurements of the intensities of light emitting diodes (LED) [22]. The first LED was developed as early as in 1962 based on a GaAsP crystal [23]. In 1971 and 1973, green [24] and yellow [25] LEDs were also developed. Because of their low efficiencies, LEDs were used only as small signal lights for a couple of decades until the first candela-class blue LED [26] and the high-brightness LEDs emitting colors from red to yellow [27] were developed. These LEDs were based on $\text{In}_x\text{Ga}_{1-x}\text{N}$ and $(\text{Al}_y\text{Ga}_{1-y})_{0.5}\text{In}_{0.5}\text{P}$ material systems, which are the most commonly used semiconductor materials in today's visible LEDs, emitting colors from blue to green and colors from yellow to red, respectively. After the development of the first blue LED, LEDs have become more potential light sources in the broad lighting application field [28-30], because the first white LED based on a blue LED chip and on broadband yellow phosphor was developed pretty soon [31]. Phosphor-coated white LEDs have been developed as well using a UVLED [32] or using other types of phosphors [33-37]. Other techniques to implement white LEDs include combining different colors emitted from different semiconductor chips, e.g. green, red and blue LEDs, [38] or using a single chip layered with several semiconductor materials to achieve many ordinary emission spectra for producing finally white light [39]. Using LEDs, it is possible to get notable energy savings if the high LED efficiency values obtained in laboratory conditions are managed to be realized in practical applications. Other advantages are the versatile spectral properties of the lighting units implemented with LEDs [40]. They enable completely new kinds of lighting systems, e.g., indoor lighting with adjustable color temperature. LEDs can be used to develop advanced radiometric applications with spectrally tunable sources [41-43].

Because the properties of the LEDs deviate quite a lot from those of the traditional light sources, new measurement techniques in photometry and colorimetry for the LEDs are needed [44-51]. LEDs often have narrow light beams [52] that complicate measurements of LED intensities. Also, the mechanical symmetry axis of the LED often diverges from its optical symmetry axis [22,53]. Other problems with LEDs are the obscurity of the size and location of the emitting surface [54,55] and the uncertainty of the far field region of the LED radiation, because LEDs are frequently equipped with lenses, or their packages may work as lenses [56]. In other words, it is difficult to know where the radiation pattern starts to be dependent of distance and where the intensity stays constant [57]. In [58-60], the distance dependence of the beam width of spatially partially coherent light sources such as LEDs has been modeled for a planar source and

even for a volumetric source. Due to the possible imaging of the physical LED source, the LED must be considered as an extended source. The inverse-square law of distance for irradiance/ illuminance does not hold up anymore.

LEDs may be modulated at high frequencies producing ultra short light pulses which are utilized, e.g., in fluorescence lifetime optical sensors [61]. On the other hand, better reliability for LEDs can be achieved with pulsed current [62] because of the reduced degradation and the lowered junction temperature. The most common method to dim LEDs is the pulse-width modulation (PWM), where the control of the light output is based on time averaging of the light signal. The use of pulsed current for dimming LEDs is based on the fact that the modulation frequency is sufficiently high as compared to the perception limit of single light pulses by a human eye which is 60 frames per seconds. Benefits of the PWM are good color stability and linearity of the brightness control that are worse in the constant current reduction method. Frequently, it is assumed that pulsing LEDs does not have any influence on the emission spectrum, because LEDs are flickered so quickly that the LED temperature is constant. At very low duty cycles, of the order of a couple of parts per thousand, an LED is assumed to be at the ambient temperature. However, LEDs driven at continuous currents are hotter. It is probable that the LED temperature changes somehow gradually between these cases.

1.2 SCOPE AND CONTENTS OF THE THESIS

In this thesis, the distance dependences of the LED illuminance and spectroradiometer signal are studied [P1-P4]. For that purpose, accurate model equations for irradiance/illuminance in the case of parallel source-detector pair with non-ideal angular characteristics are derived [P2,P4]. Because the model equations include information about the directivities of the source and detector, the angular characteristics of the sources and detectors used are experimentally measured [P1], and modeled with cosine power-law functions [P2]. Their spatial characteristics are also measured, and modeled by polynomial functions. The new model equations with characterized parameters are applied to investigate the optical receiving planes of spectroradiometer diffusers [P2], and the luminous intensities of standard lamps and LEDs [P3,P4].

Experimental set-ups for measuring the positions of the optical receiving planes and the angular responsivities of four spectroradiometer diffusers at four wavelength bands are constructed [P1]. The reference plane displacements of the diffusers are determined as the distances between the outermost surfaces and the measured optical receiving planes of the diffusers [P1]. To take into account the diffuser reference plane shifts in the calibrations of spectroradiometers, a multiplicative correction factor for the earlier measurement data is presented [P2].

A novel method for analyzing LEDs is developed [P3]. The method consists of irradiance/illuminance measurements at various distances from the LED, angular distribution measurements, and fitting of the derived model equation [P4] to the measurement data using the size and location of the LED source as free parameters. The method is demonstrated for the luminous intensities of 17 LEDs with different packages, angular distributions, and power levels [P3]. For choosing the appropriate distance measurement ranges, also the site on the measurement axis beyond the beam widths of the studied LEDs remain constant are determined.

Spectral, thermal, and color behaviors of three commercial AlGaInP [P5] and InGaN low-power LEDs under the PWM dimming are also studied. The emission spectra with different duty cycles of LEDs are recorded. The peak wavelengths, bandwidths and color coordinates of the LEDs are determined from the recorded spectra. An explanation for the spectral changes of the AlGaInP LEDs during the PWM control is developed and tested [P5]. Junction temperatures and charge carrier temperatures of LEDs in the PWM control are measured for the first time [P5]. Changes in the colors of the pulsed LEDs are observed. Some recommendations for the users and manufacturers of LEDs related to the optimal use of LEDs and to making datasheets are given.

1.3 CONTRIBUTION OF THE RESEARCH

The thesis contains the following new scientific results:

- 1) Irradiance equations for measurement geometries with a highly directional, non-uniform source and detector have been derived.

- 2) A new effect, reference plane displacement, on entrance diffusers of spectroradiometers has been detected. The displacement has been observed to be a function of wavelength and non-zero even in the case of planar diffusers. A correlation between the reference plane offsets and cosine responses of the planar diffusers has been found.
- 3) A novel method for analyzing the luminous/radiant intensity of an LED has been developed. The method produces consistent intensity values at a large distance range. As a spin-off, information about the dimensions of the virtual LED source is obtained.
- 4) The blueshift in the peak wavelength and the bandwidth narrowing in the emission spectra of low-power LEDs under the PWM dimming have been found. The junction temperatures of the AlGaInP LEDs were observed to change linearly during the PWM dimming. Apparent color variations perceived by the human eye were observed for two AlGaInP LEDs under the PWM control.

2 MODELING ENERGY TRANSFER BETWEEN PARALLEL PLATES

Energy transfer between two parallel plates having various geometries has been studied in several papers [63-66] but, so far, the solution for the case, where a directional source or detector with non-uniform spatial characteristics would be considered, has not been published. A complex integral of the energy transfer between radiating rectangular/circular and detecting circular parallel plates with non-cosinusoidal angular characteristics was solved in [P2,P4]. The new model equation was applied to determine the irradiance at varying distances from a source.

In section 2.1, the model equation derived in [P2] for analyzing the reference plane offset of the diffuser is presented in such a way that the shapes of the spatial characteristics of the source and detector, and the deviation of the center of the light source from the measurement axis are taken into account. In section 2.2, another model equation that was applied to the LED intensity analysis in [P3] is presented in more generic form than in [P4].

2.1 MODEL EQUATIONS FOR INCANDESCENT LAMPS

2.1.1 *Comprehensive equation*

Consider such a measurement geometry where an off-centered, rectangular emitting surface with width x_0 and height y_0 and a receiving aperture of a circular detector with radius r_0 are parallel at distance D from each other (Figure 1). The z axis of the coordinate system crosses the center of the detector while it is shifted by $y_0(0.5 - a)$ from the center of the emitting surface.

The signal dS of a detector surface element dA_D at (r, φ, D) produced by a small surface element dA_S at $(x, y, 0)$ is given by

$$dS = R(r, \varphi; \theta) L_e(x, y; \theta) dA_{\perp} d\Omega \quad (1)$$

where $R(r, \varphi, \theta)$ is the flux responsivity of the detector in incidence direction θ at surface element dA_D , $L_e(x, y; \theta)$ is the radiance of the source at surface element dA_S in direction θ , $dA_{\perp} = dA_S \cos \theta$ is the projected area of dA_S , and $d\Omega = dA_D \cos \theta / D_S^2$ is the solid angle from the point $(x, y, 0)$ to the surface element dA_D . The distance between area elements dA_S and dA_D is $D_S = [D^2 + (x - r \cos \varphi)^2 + (y - r \sin \varphi)^2]^{1/2}$.

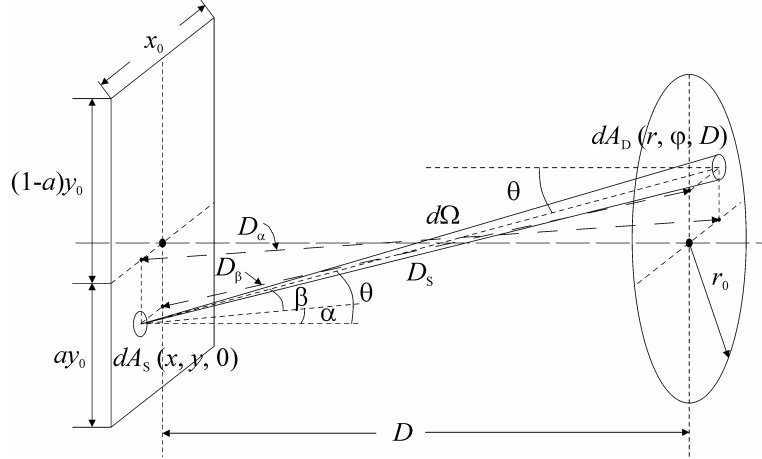


Figure 1. Geometrical parameters for the energy transfer integral in the case of off-centered rectangular and symmetric circular parallel plates.

The radiance of the source,

$$L_e(x, y; \alpha, \beta) = L_0 L(x, y) \frac{I(\alpha, \beta)}{\cos \alpha \cos \beta}, \quad (2)$$

has the normalization term L_0 , spatial distribution $L(x, y)$, and angular dependence factor $I(\alpha, \beta) / \cos \alpha \cos \beta$. Equation (2) presumes that the angular and spatial distributions do not depend on each other. The angular distribution of the source is described by [P2]

$$I(\alpha, \beta) \approx \left(1 - \frac{1}{2} p \alpha^2\right) \left(1 - \frac{1}{2} q \beta^2\right) \approx \cos^p \alpha \cos^q \beta, \quad (3)$$

where the normalized angular distribution $I(\alpha, \beta)$ of the source is modeled by two parabolic curves in horizontal and vertical directions within a few degrees around the optical axis. Parameters p and q are the directivities of the source in horizontal and

vertical directions, respectively. When $p = q = n$, equation (3) is reduced to $I(\alpha, \beta) = \cos^n \theta$, where $n = 1$ for a Lambertian source.

The spatial distribution of the radiance can be approximated by a quadratic polynomial function

$$L(x, y) = k_0 + k_1 y + k_2 y^2, \quad (4)$$

where factors k_i are the coefficients of the polynomial describing the radiance distribution in the direction of the y axis. For a simplification, it is assumed that the radiance does not depend on x . $L(x, y)$ is normalized to unity, then $k_0 = 1$. The normalization factor L_0 can be determined by integrating the spatial distribution of the radiance over surface elements dA_s

$$L_0 = \frac{I_0}{\int_{-ay_0}^{(1-a)y_0} \int_{-x_0/2}^{x_0/2} L(x, y) dx dy} = \frac{I_0}{x_0 y_0 \left\{ 1 + \frac{k_1}{2} (1-2a)y_0 + \frac{k_2}{3} [(1-a)^3 + a^3] y_0^2 \right\}}, \quad (5)$$

where I_0 is the radiant intensity of the source. If the source is homogeneous ($k_1 = k_2 = 0$), the normalization simplifies to $L_0 = I_0 / (x_0 y_0)$.

The radiant flux responsivity $R(r, \varphi, \theta)$ of a detector,

$$R(r, \varphi; \theta) = R_\phi R(r, \varphi) \frac{K(\theta)}{\cos \theta}, \quad (6)$$

depends on the flux responsivity R_ϕ , normalized spatial responsivity $R(r, \varphi)$, and angular dependence factor $K(\theta) / \cos \theta$. A similar assumption on separateness in equation (6) is made as in equation (2). Rotational symmetry is assumed in the spatial and angular responsivities. Normalized angular responsivity $K(\theta)$ can be approximated by a parabolic curve within a few degrees from the normal of the surface element dA_D ,

$$K(\theta) \approx 1 - \frac{1}{2} m \theta^2 \approx \cos^m \theta, \quad (7)$$

where m is the directivity of the detector. Then the flux responsivity of the detector with ideal, cosinusoidal angular responsivity ($m = 1$) does not depend on θ .

The spatial non-uniformities in the detector responsivities can be treated in the same way as with the source. The spatial responsivity of the detector is described by a polynomial function of N^{th} degree given by

$$R(r) = \sum_{i=0}^N c_i r^i \quad (8)$$

with coefficients c_i . Because $R(r)$ is dimensionless, it follows that $c_0 = 1$. The flux responsivity R_Φ can be expressed with irradiance responsivity R_E by integrating equation

$$R_\Phi = \frac{R_E}{\int_0^{r_0} \int_0^{2\pi} R(r) d\varphi dr} = \frac{R_E}{2\pi \left(\sum_{i=0}^N \frac{c_i}{i+2} r_0^{i+2} \right)}, \quad (9)$$

where r_0 is selected so that $R(r=r_0)$ is approximately zero. If the response of the detector is spatially uniform and $N=0$, equation (9) is reduced to form $R_\Phi = R_E / (\pi r_0^2)$.

On the basis of the approximation derived for the denominator of the energy transfer integral in [P2] and the used formulae for geometric parameters in Figure 1, the total irradiance signal $E_e(D)$ as a function of distance can be expressed in the form

$$\begin{aligned} E_e(D) = & \frac{L_0}{D^2} \frac{R_\Phi}{R_E} \int_{-ay_0}^{(1-a)y_0} \int_{-\frac{x_0}{2}}^{\frac{x_0}{2}} \int_0^{r_0} \int_0^{2\pi} (1 + k_1 y + k_2 y^2) \left(\sum_{i=0}^N c_i r^i \right) \times \\ & \times \left[1 + \frac{p}{2D^2} (x^2 - 2rx \cos \varphi + r^2 \cos^2 \varphi) \right] \left[1 + \frac{q}{2D^2} (y^2 - 2ry \sin \varphi + r^2 \sin^2 \varphi) \right] \times \quad (10) \\ & \times \left[1 + \frac{m+2}{2D^2} (r^2 + x^2 + y^2 - 2rx \cos \varphi + 2ry \sin \varphi) \right] d\varphi dr dx dy . \end{aligned}$$

This can be integrated in a straightforward way and when the reverse series expansion for the integration result (see [P2]) is made, the equation for the distance dependence of the irradiance signal can be stated as

$$E_e(D) \approx \frac{I_0}{D^2 + r_s^2 + r_D^2}, \quad (11)$$

where the modified radius parameters are defined by the equation

$$\begin{bmatrix} r_s \\ r_D \end{bmatrix} = \frac{1}{2} \begin{bmatrix} \sqrt{\frac{m+p+2}{6} x_0^2 + 2(m+q+2) \frac{F_{S2}}{F_{S1}} y_0^2} \\ r_0 \sqrt{\left(m + \frac{p+q}{2} + 2\right) \frac{F_{D2}}{F_{D1}}} \end{bmatrix} \quad (12)$$

and the spatial responsivity and distribution terms are given by

$$\begin{aligned} F_{S1} &= \sum_{i=0}^2 \frac{k_i}{i+1} \left[(1-a)^{i+1} - (-a)^{i+1} \right] y_0^i \\ F_{S2} &= \sum_{i=0}^2 \frac{k_i}{i+3} \left[(1-a)^{i+3} - (-a)^{i+3} \right] y_0^i \\ F_{D1} &= \sum_{i=0}^N \frac{c_i}{i+2} r_0^i \\ F_{D2} &= 2 \sum_{i=0}^N \frac{c_i}{i+4} r_0^i \end{aligned} \quad (13)$$

In equation (11), terms of order x^4/D^4 , y^4/D^4 , r^4/D^4 , etc. are omitted. Finally, radiometric quantities E_e and I_0 can be transformed into the corresponding photometric quantities E_v and I_v by $V(\lambda)$ -weighted integration.

The modified radius parameters shown in equation (12) contain the factors from the angular and spatial distributions of the source, the angular and spatial responsivities of the detector and the optical axis deviation relative to the center of the source in the direction of the y axis. The first terms including the directivities of the source and detector in equation (12) signify that an optical detector averages the non-uniform irradiance in the detector aperture plane. Irradiance decreases on the edges of the detector aperture as the directivities of the source and detector increase and, thus, the averaging effect of the detector becomes more emphasized. The factors of the modified radius parameters stated in equation (13) take into account the effective position of the center of the source relative to the measurement axis and the shape of the spatial responsivity curve of the detector. Factor F_{S2}/F_{S1} is significant when the maximum of

the radiance distribution is located relatively far away from the optical axis, which is probable when parameter a differs relatively much from the value of $1/2$.

2.1.2 Simplified equations

For the symmetric, uniform source, $L(x, y) = 1$ and $a = 1/2$, the source factors in equation (13) are reduced to $F_{S1} = 1$ and $F_{S2} = 1/12$. Correspondingly, if the detector responsivity is uniform over the aperture surface, or $R(r) = 1$, $F_{D1} = 1/2$ and $F_{D2} = 1/2$. In that case, the modified radius parameters of equation (12) are simplified to [P2]

$$\begin{bmatrix} r_S \\ r_D \end{bmatrix} = \frac{1}{2} \begin{bmatrix} \sqrt{\frac{m+p+2}{6}x_0^2 + \frac{m+q+2}{6}y_0^2} \\ r_0 \sqrt{m + \frac{p+q}{2} + 2} \end{bmatrix}. \quad (14)$$

When the source and detector also have cosinusoidal angular characteristics, or $m = p = q = 1$, the radius parameters are of the form [P2]

$$\begin{bmatrix} r_S \\ r_D \end{bmatrix} = \begin{bmatrix} \sqrt{\frac{x_0^2 + y_0^2}{6}} \\ r_0 \end{bmatrix}. \quad (15)$$

In [P1], the rectangular source was modeled by a circular source of the same area. Then the effective radius parameter r_0' of the source is modified to $(x_0 y_0 / \pi)^{1/2}$. For the point source and point detector, equation (11) gets a simple form $E_e = I_0 / D^2$.

2.2 MODEL EQUATIONS FOR DIODE EMITTERS

Measuring the intensity of LEDs corresponds more or less to the case presented above. The main difference from the previous case is that both plates can be assumed to be circular and symmetric. Because in the measurement of LED intensity, obtainable source dimensions are approximative [P3], it is convenient to assume that the LED source is homogeneous and it has rotationally symmetrical angular distribution and, also, the optical axis crosses the centers of the circular plates. Figure 2 describes geometrical parameters in the derivation of the model equation.

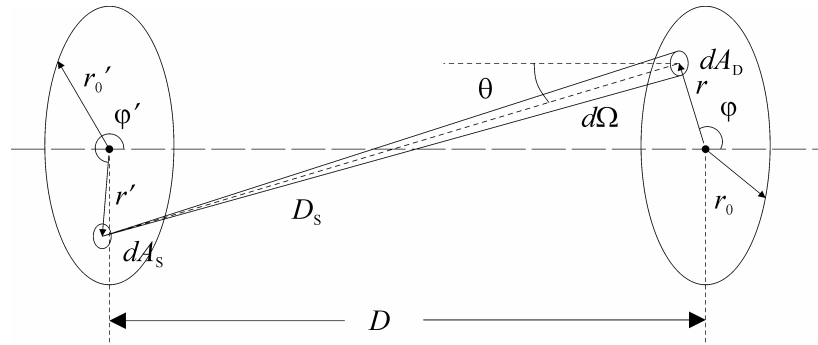


Figure 2. Geometrical parameters in the case of two circular parallel plates.

The radiance/luminance of the source can now be expressed in the form

$$L_{e/v}(r, \varphi; \theta) = \frac{I_{e/v, \text{eff}}}{\pi r_0'^2} \frac{I(\theta)}{\cos \theta}, \quad (16)$$

where $I_{e/v, \text{eff}}$ is the effective radiant/luminous intensity of an LED and r_0' is the radius of the source and the angular distribution is

$$I(\theta) = \cos^n \theta. \quad (17)$$

Then, the energy transfer integral can be presented in the form [P4]

$$E_{e/v}(D) = \frac{I_{e/v, \text{eff}}}{\pi^2 r_0'^2 r_0^2} \int_A \int_{A'} \frac{\cos^{m+n} \theta dA dA'}{D_s^2}, \quad (18)$$

where the slant distance is $D_s = [D^2 + r^2 + r'^2 - 2rr' \cos(\varphi - \varphi')]^{1/2}$. As equation (16) is integrated by the means of [P4], the final irradiance/illuminance,

$$E_{e/v}(D) \approx \frac{I_{e/v, \text{eff}}}{D^2 + r_s^2 + r_D^2} g(D), \quad (19)$$

is given in terms of the modified radius parameters of the source and detector

$$\begin{bmatrix} r_s \\ r_D \end{bmatrix} = \frac{\sqrt{m+n+2}}{2} \begin{bmatrix} r_0' \\ r_0 \end{bmatrix} \quad (20)$$

and the multiplication factor

$$g(D) = \frac{2}{1 + \sqrt{1 - 4r_S^2 r_D^2 / (D^2 + r_S^2 + r_D^2)^2}}. \quad (21)$$

For the source and detector with cosinusoidal angular characteristics, the $g(D)$ factor is very close to unity and equation (19) can then be reduced to the form

$$E_{e/v}(D) = \frac{I_{e/v,\text{eff}}}{D^2 + r_0^2 + r_0^2}. \quad (22)$$

3 MODELING STANDARD LAMPS

The radiance and temperature distributions of various lamp filaments have been observed to be non-uniform [67-70]. Also, it has been noted that helical filaments of FEL lamps are not necessarily uniformly threaded. Due to these effects, the radiance distribution of a FEL lamp can have an unexpected shape. Alignment jigs of FEL lamps have been designed for reproducible measurements and aimed that the optical axis of the measurement system determined by the jig travels the center of the lamp filament. However, it is noted that the optical axis does not cross the filament center in the vertical direction. In this section, parameters related to these effects, which were taken into consideration in the previous section, are determined for three lamps. Also, directivities of the same lamps are measured. One of the lamps is a 180-W Osram Wi41/G lamp from PRC Krochmann GmbH and the other two ones are 1-kW FEL lamps of type BN-9101 from Gigahertz Optik (see Figure 3). The BN-9101-313 (hereafter FEL-313) lamp is a spectral irradiance standard lamp and it is used as a light source in the diffuser offset determination of section 4.3. The BN-9101-391 (hereafter FEL-391) and Wi41/G lamps are luminous intensity standard lamps. Luminous intensity standard lamps are usually calibrated by measuring the illuminance at one, relatively large distance [71-77]. In this section, also the accuracy of the point approximation for analyzing the luminous intensities of these two lamps are investigated with the new model derived in section 2.1.

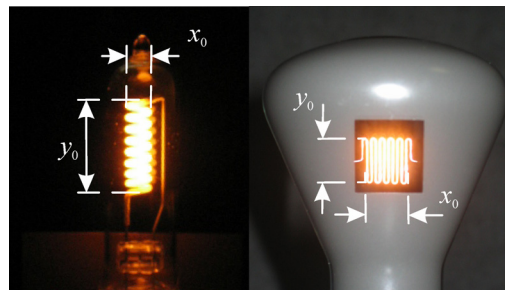


Figure 3. Standard lamps of types BN-9101 (on the left) and Wi41/G (on the right). The dimensions of the lamps are: $x_0 = y_0 = 15$ mm (Wi41/G), and $x_0 = 5$ mm and $y_0 = 18$ mm (BN-9101) [P2].

3.1 DIRECTIVITY PARAMETERS

Directivities p and q of a FEL lamp in equation (3) were determined on the basis of the intensity distribution graph presented in [78] for a lamp of the same type. Corresponding parameters of the Wi41/G lamp were determined with the illuminance distribution measured at a distance of 0.7 m on the perpendicular plane that was transformed into angular intensity distribution $I(\alpha, \beta)$ using the cosine-cubed law [64, 78]. The values of directivity parameters p and q were determined by fitting curves $\cos^p(\alpha-\alpha_0)$ and $\cos^q(\beta-\beta_0)$ to the measured data points in horizontal and vertical directions by varying parameters p and q and angular offsets α_0 and β_0 . The angular distributions in the horizontal and vertical directions and the fits to them are shown in Figure 4. The fitting results were obtained to be $p = 0.0$ and $q = 5.0$ for the FEL lamp and $p = 7.6$ and $q = 9.3$ for the Wi41/G lamp. FEL types of lamps work as isotropic radiators in the horizontal plane due to the cylindrical structure of the filament.

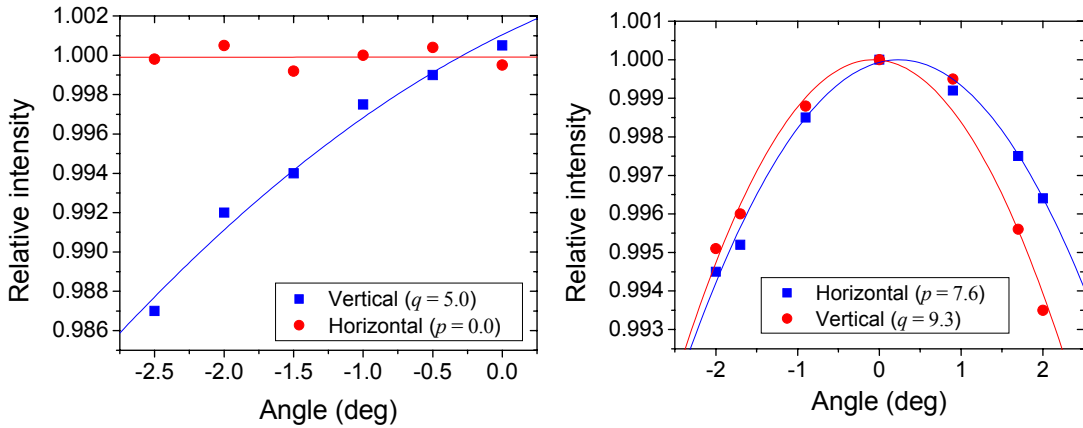


Figure 4. Fits of $\cos^p \alpha$ and $\cos^q \beta$ curves to angular distributions of FEL lamp (on the left) [78] and Wi41/G lamp (on the right).

3.2 RADIANCE DISTRIBUTION AND OFF-CENTRICITY

The luminance distributions of the FEL lamps were measured in the y direction with a luminance meter in such a way that the measurement area in the filament was a circle, whose diameter was the same as the width $x_0 = 5$ mm of the filament. The luminance values were recorded by steps of 2 mm from the lower part of the filament to the upper part. For the FEL-313 lamp, a linear slope and the value of $k_1 = 13.2 \text{ m}^{-1}$ were obtained.

The luminance distribution of the FEL-391 lamp was modeled by a parabolic curve (see Figure 5).

Location of the optical axis below the center of the lamp filament is demonstrated with the photograph in Figure 5. For the photograph, the FEL-391 lamp was aligned with the alignment jig of the lamp using a red alignment laser. The value of parameter a [see Figure 1 and equation (13)] for the FEL-313 lamp was $2/5$, then the optical axis determined by the alignment jig was located 1.8 mm below the center of the filament. The corresponding values for the FEL-391 lamp were $a = 3/10$ and 3.6 mm.

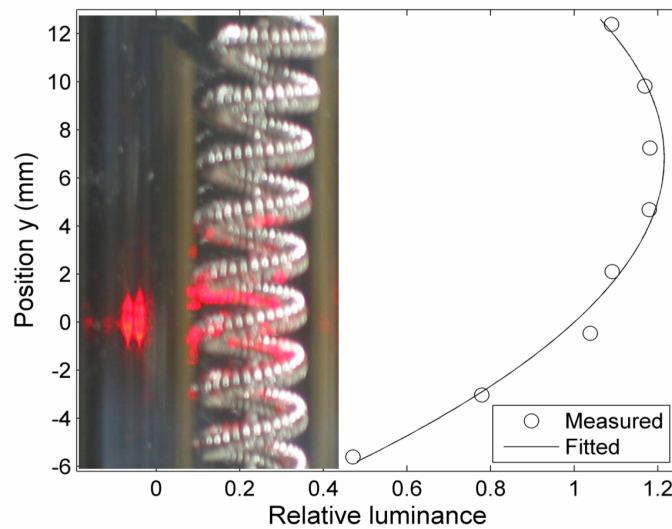


Figure 5. Luminance distribution of lamp FEL-391 together with the photograph showing the optical axis location relative to the filament. The red light comes from the alignment laser beam whose center marks the position of the optical axis.

The radiance distribution of the Wi41/G lamp is assumed to be uniform due to the horizontal filament structure of the lamp [$L(x, y) = 1$]. On the basis of visual observation, the measurement axis crosses the center of the lamp filament ($a = 0.5$). Then, the simplified radius parameters of equation (14) may be used in equation (11).

3.3 ACCURACY OF THE LUMINOUS INTENSITY ANALYSIS

The luminous intensity values were simulated with equations (11–13) for the FEL-391 lamp, with equations (11) and (14) for the Wi41/G lamp, and with the inverse-square

law of the point source and detector (see section 2.1.2) for both lamps. The values of the lamp parameters determined in two previous sections were used in these model equations. To find out the accuracy of the point source and point detector approximation in the analysis of the luminous intensity standard lamps, the simulated luminous intensity values calculated with the new model and the point approximation were compared at different distances. The investigation was made with two spatially uniform detectors whose directivity parameter m and the size of the detector aperture differed from each other. The results from the comparison of the luminous intensities calculated with two methods are shown in Figure 6. The results indicate that at short distances, less than 1 m, the deviation of the point approximation from the accurate model is quite large as compared to the uncertainty component of distance setting in luminous intensity measurements which is usually a couple of parts in 10^4 .

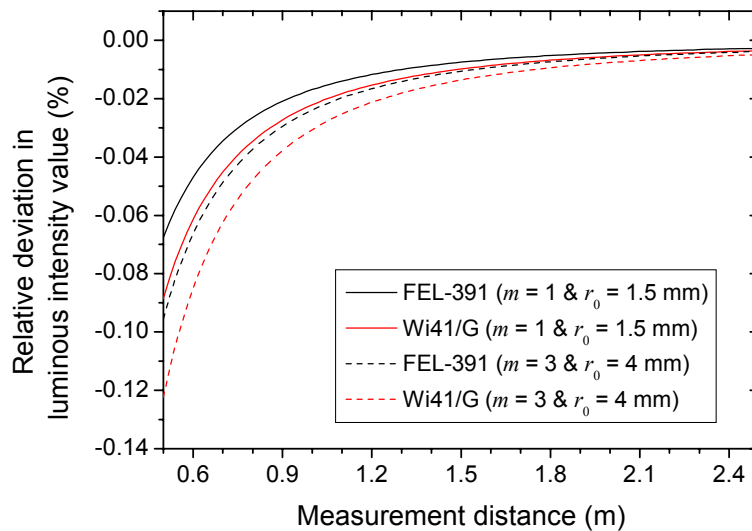


Figure 6. Accuracy of the point approximation in the luminous intensity analysis of the Wi41/G and FEL-391 lamps at different distances.

4 OPTICAL CHARACTERIZATION OF DIFFUSERS

Transmission diffusers are used as entrance optics in various detectors where cosinusoidal detection in terms of incidence angle is required. When illuminating an ideal diffuser with a homogeneous plane wave, its rear surface radiates the light as the cosine of the incident angle of its front surface. In practical devices, light is then coupled either into an optical fiber (spectroradiometers) or a filtered radiometer (broadband UV meters and luxmeters). The diffuser is in practice designed so that its shape, thickness and material are optimized to achieve good cosine response and sufficient sensitivity for an instrument [10-12,79]. The position of the optical receiving plane of the diffuser has not been much under consideration. In this section, the optical properties of spectroradiometer diffusers are determined especially concentrating on the determination of the position of the optical receiving plane [P1,P2]. Three flat diffusers of types Bentham D3, D5, and D7 and one dome-shaped diffuser of type Schreder J1002-01 (see Figure 7) are studied. All of these diffusers have been designed to be installed onto an optical fiber bundle.

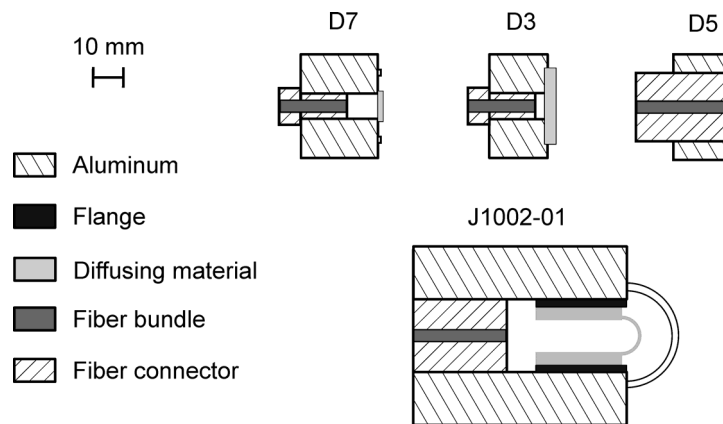


Figure 7. Indicative sketches of the studied diffusers. The ratios of the dimensions correspond to the actual diffusers.

4.1 ANGULAR RESPONSIVITIES

Matching the angular responsivity of a spectroradiometer to the cosinusoidal response is one of the most critical issues when measuring global solar irradiance. The global irradiance consists of a large diffuse radiation component in addition to the direct radiation component from the sun. The diffuse radiation is due to scattering by air molecules and aerosols and it falls on the surface of the earth everywhere from the half-space. This scattering is of Rayleigh type and the diffuse component of the solar irradiance is significant relative to the direct component particularly in the UV region. Because an ideal cosine-diffuser cannot be realized, the measured global irradiance values may be corrected with the known angular responses of the diffuser. [80-84]

The angular responsivities of each of four diffusers studied were determined using a turntable [P1]. Each diffuser had unique angular responsivity curves in terms of the quality of the cosine response (see Figure 8) and the wavelength dependence. In Figure 9, the angular responsivity curves of diffuser D5 are normalized at high incidence angles to demonstrate the explanation of the angular responsivity effect of the diffuser. Transmitted light after the diffusing plate of the D5 includes both the direct and diffuse transmission components the ratio of which increases as a function of wavelength. At large angles, diffuser D5 has quite good cosine response due to its diffuse transmission component, but at small angles the direct component dominates due to the transparency of the diffuser at near-infrared (NIR) wavelengths.

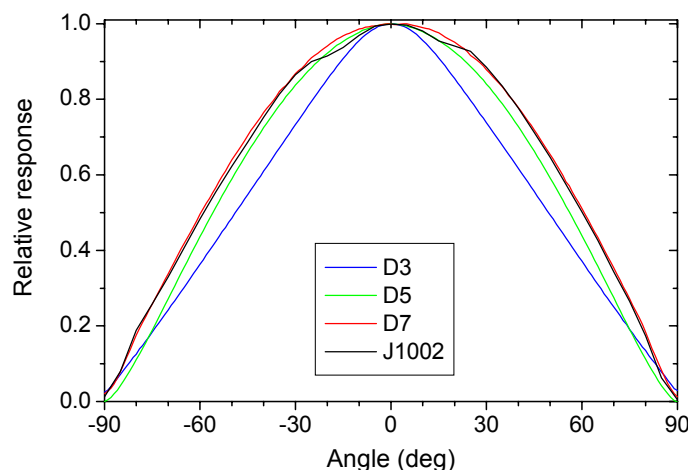


Figure 8. Angular responsivities of the diffusers at the UVA band.

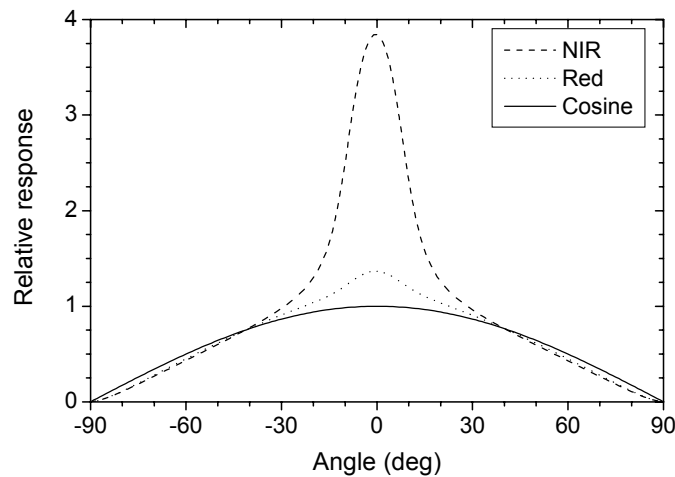


Figure 9. Angular responsivity of diffuser D5 at two wavelength bands.

The values of directivity parameter m in equation (7) for the diffuser offset analysis of the studied diffusers were determined by fitting the $\cos^m(\theta-\theta_0)$ curve to the measured angular responsivity data of the diffusers by using m and angular offset θ_0 as free fitting parameters. [P2]

4.2 SPATIAL RESPONSIVITIES

The spatial responsivities of diffusers are usually assumed to be uniform. However, diffusers of a Brewer spectroradiometer [85] and broadband UV radiometers [86,87] have been observed to couple the incoming radiation significantly more from the center of the diffuser than from the edges. Therefore it was of interest to investigate where from the diffusing plate of the studied diffusers the signal gets into the optical fiber [P2]. The spatial responsivities of the studied diffusers were recorded by scanning the diffusing plate at two perpendicular directions using a linear translator and lasers emitting at wavelengths of 325 nm, 543 nm and 633 nm.

In the results from the spatial responsivity measurements of [P2], it was noted that the spatial responsivity is the result from the geometry of the diffusing material and the distance between the diffusing plate and the entrance port of the optical fiber. The D3 diffuser, whose diffusing material is water-free quartz, scattered the light in a different way as the Teflon diffusers. The sizes of the effective receiving apertures of the D3 and D5 diffusers were roughly equal to the size of the entrance port of the optical fiber bundle (4 mm in diameter). In [P2], the sizes of the receiving apertures of the studied

diffusers were calculated on the basis of the full-widths at half maximum (FWHM) of the spatial responsivity curves. Now, the shapes of the spatial responsivities of the diffusers are taken into account in the diffuser reference plane offset analysis. The values of spatial responsivity coefficients c_i [see equations (8) and (13)] were determined by fitting an N^{th} degree polynomial function to the measurement data (see Figure 10).

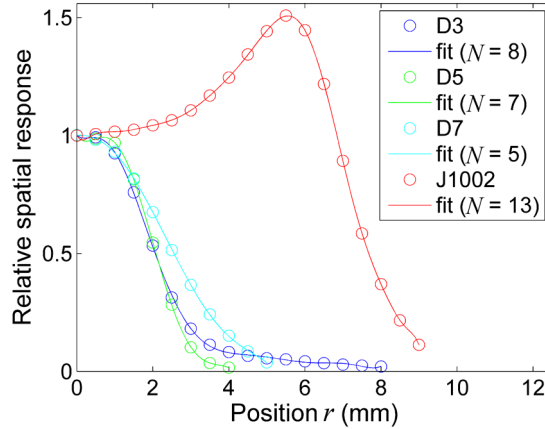


Figure 10. Fits of polynomial functions to the measured spatial responsivity curves of the studied diffusers.

4.3 RECEIVING PLANE POSITIONS

Figure 11 illustrates the main principle of the determination of the diffuser receiving aperture plane position. The diffuser offset Δd_D fixes this plane position with respect to the outermost surface of the diffuser in question. The procedure of the distance offset determination consisted of irradiance measurements at various distances d by a reference detector having a well-known aperture plane position and by a detector equipped with a diffuser. The lamp offset Δd_S fixing the effective filament position was determined from the distance dependence of the signal of the reference detector and, then, utilizing this offset, the diffuser offset Δd_D was determined from the distance dependence of the signal of the detector studied. Offsets Δd_D and Δd_S were analyzed by equations (11–13) as $D = d + \Delta d_D + \Delta d_S$. The scheme was repeated at four wavelength bands (UVA, Green, Red, and NIR) to study possible spectral features caused by the diffusing material. [P1]

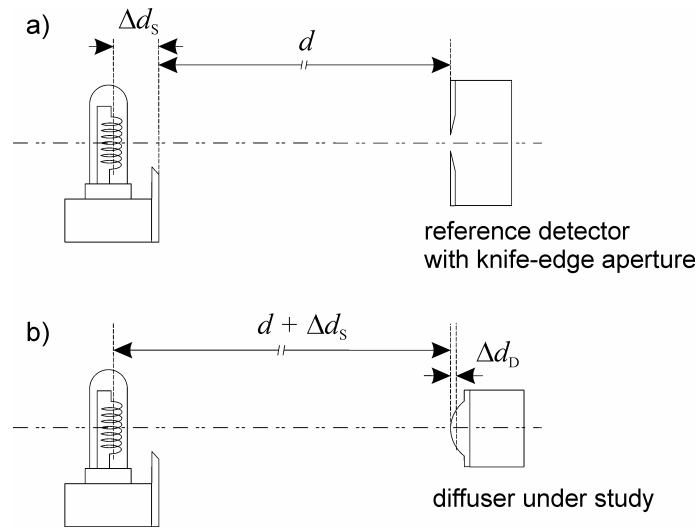


Figure 11. Illustration of the determination of the distance offsets of diffusers. **a)** Lamp offset Δd_s fixes the effective location of the lamp filament relative to the front plate of the FEL lamp. **b)** Diffuser offset Δd_D fixes the position of the effective receiving plane of the diffuser relative to its outermost surface.

4.3.1 Reference plane displacements and their significance

Results of the distance offset measurements are shown in Figure 12. Diffuser D3 has a significant offset practically independent of wavelength. Diffuser D7 has zero offset in the average in the whole range studied. The reference plane of diffuser J1002 has shifted quite a lot and weak wavelength dependence occurs. Diffuser D5 has strongly wavelength dependent offset but in the ultraviolet region the offset is almost zero. In [88], the distance offset of diffuser J1002 has been confirmed.

If a solar UV spectroradiometer with a nonzero diffuser reference plane displacement was calibrated, as usual, with respect to the outermost surface of the diffuser, systematic measurement errors would be obtained. For instance, such a calibration for a solar UV spectroradiometer equipped with the J1002 diffuser, which is carried out at a distance of 0.5 m from a spectral irradiance standard lamp (see [P2]), causes an overestimation of 2.3 % for solar UV irradiance level as measured with the spectroradiometer.

To take the offset effect into account in the calibration of the spectroradiometer, the calibration distance from the irradiance standard lamp should be determined with

respect to the plane defined by the diffuser offset. This is straightforward to accomplish in the case of diffusers with wavelength independent offsets (D3, D7, and J1002) where one single plane can be used for calibrations over quite a wide wavelength range. Challenges are encountered when calibrating, at wide wavelength region, spectroradiometers with the D5 diffuser which has spectrally varying offsets. In this case, it is easier to use a simple mathematical function to correct the wavelength dependence of the diffuser reference plane instead of using several measurement reference planes. In the case of these diffusers, the calibration of the spectroradiometer could be made first relative to one measurement plane and then, using a mathematical function modeling the reference plane as a function of wavelength, the recorded calibration data could be corrected [P2]. The correction factor may be used not only for correcting the calibration data at other wavelengths, but also for earlier irradiance measurement results obtained with respect to an erroneous reference plane position.

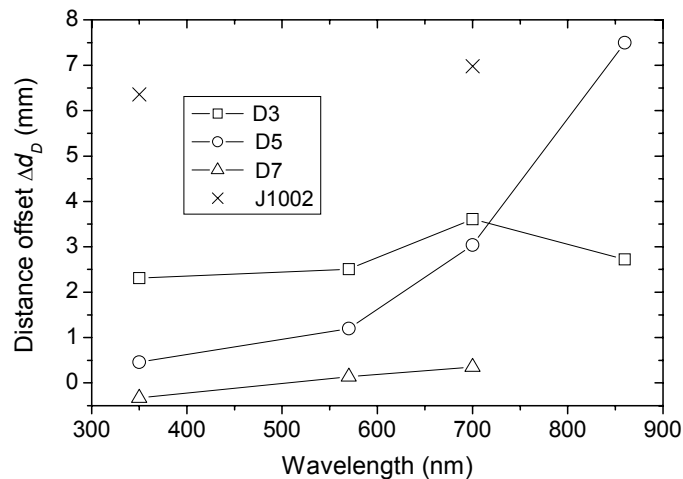


Figure 12. Distance offsets of the diffusers as a function of wavelength.

4.3.2 Evaluation of measurement need

The results, which indicate obvious reference plane displacements in most cases, suggest that systematic measurement errors may be present in the measurement data obtained earlier with incompletely calibrated spectroradiometers. The new method gives a good estimate for the diffuser reference plane position at various wavelengths [P1,P2]. The determination of the diffuser reference plane position includes quite a lot of measurements, thus it is appropriate to evaluate the need for determining the location of this plane before starting measurements.

If the diffuser is dome-shaped, it is obvious that the effective receiving aperture is located inside the diffuser. In [21], distance offsets were calculated from the geometry and it was noted that the diffuser reference plane displacement is significantly underestimated with pure geometrical consideration. The refraction of light in the diffusing material should be combined for appropriate geometrical correction. This is a demanding task. Earlier measurement results suggest that especially the distance reference plane position of the dome-shaped diffusers should be experimentally determined [P1,21].

In the case of flat diffusers, a clear correlation between the wavelength dependences of the distance offsets and angular responsivity curves occurred. Hence, it was of interest to study the correlation more in detail. Figure 13 presents the correlation between the angular responsivity at 30° angle and the distance offsets of the planar diffusers. Because the solar UV measurement stations typically have much angular responsivity data available for their spectroradiometers, Figure 13 gives useful information about the need for measuring the diffuser reference plane position. The lower the deviation from the cosine response, the smaller the distance offset, and thus there is less need for carrying out the characterization measurements of the reference plane position.

4.3.3 *Simplification of the analysis model*

A complete analysis of diffuser reference plane requires a large amount of work. It is of interest to investigate whether certain analyses can be excluded, and how large errors are induced by the simplifications. The angular and spatial characterizations of the source and detector need an x-y linear translator, a turntable and different types of detectors like irradiance and radiance detectors. The distance and irradiance measurements are inevitable but the measurement needs of the spatial and angular characteristics of the source and detector may be reduced in some cases.

In [P2], four cases for approximating the modified radius parameters in the analyses of the distance offset and the correction factor were presented and tested. Approximation errors for the distance offsets of all diffusers except the D5 diffuser at the 700 nm and 860 nm bands were smaller than 0.15 mm [P2]. Figure 14 shows the approximation errors in the distance offset values of the D5 diffuser. Cases 1-3 (see Table 3 of [P2]) used for the correction factor were valid with an accuracy of 0.3 % as compared to Case

4 [equation (14)]. Neglecting the shape of the spatial characteristics of the detector and source in equation (12), which corresponds to equation (14), causes an error smaller than 0.1 mm for the offset value in all cases of the studied diffusers. An offset error caused by that effect for diffuser D5 at the NIR band was 0.09 mm, and corresponding errors for the J1002 diffuser at the UVA and Red bands were 0.05 mm and 0.06 mm. All-inclusive characterization of the measurement system needed for the use of the accurate model equations is of importance when a diffuser has a sharp angular responsivity, a large diffusing plate, and a non-uniform spatial responsivity. [P2]

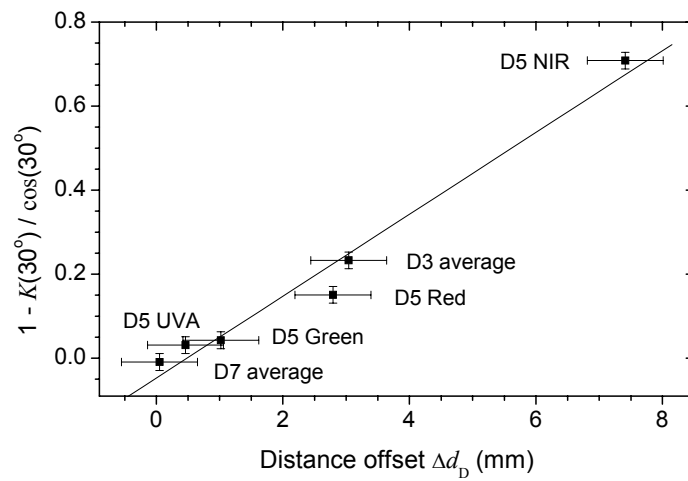


Figure 13. Comparison of offsets of planar diffusers with their $K(\theta = 30^\circ)$ values. To illustrate the correlation, the trend line is presented.

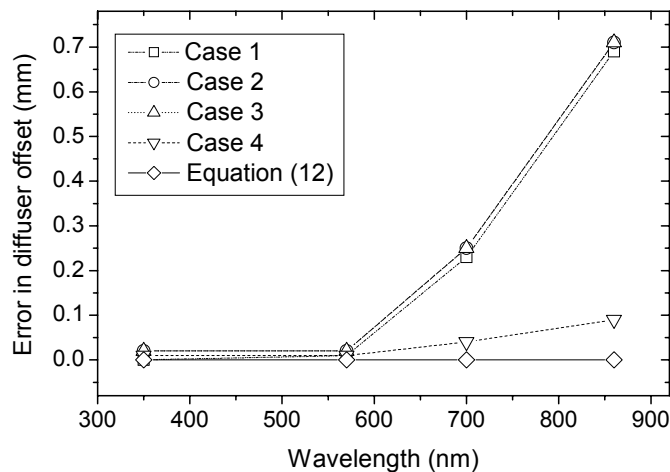


Figure 14. Approximation errors of the distance offsets of the D5 diffuser as a function of wavelength (see [P2] for details).

5 ANALYZING INTENSITY OF DIODE EMITTERS

In LEDs, light is produced by spontaneous emission in the light-emitting region of the semiconductor chip. The emitting region may be considered as a Lambertian light source. To get better efficiency, LEDs are equipped with reflector cups [89], encapsulating lenses [56] and chip modifications including roughening [90] and shaping [91]. Thus radiometric measurement problems are met, because LEDs do not necessarily work anymore as Lambertian sources, but rather as highly non-Lambertian, directional sources [P3] (see Figure 15).

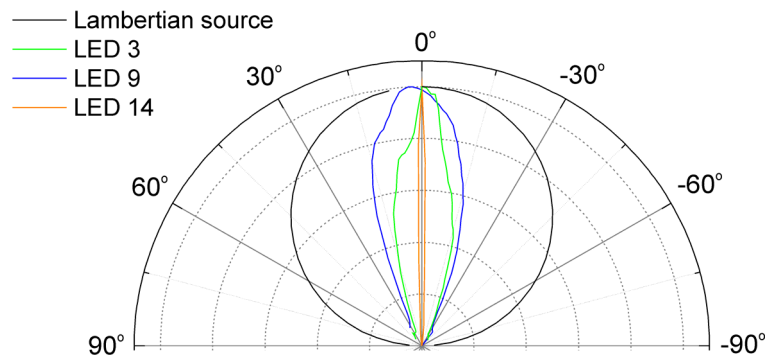


Figure 15. Comparison of the angular distributions of three LEDs to that of the Lambertian source. (see [P3] about numbering of LEDs)

A couple of different methods have been developed for measuring the position of the LED source which anyway necessitate information about the emitting area of the LED source and ignore the LED directivity [55,92]. In [P3], luminous intensity analysis of several LEDs was carried out by using the conventional inverse-square law. The results indicate that many LEDs had distance dependent luminous intensities even when the position of the LED source was freely varied [P4]. This was the case for the results analyzed by the CIE method [22] as well [P3,93]. To overcome these problems, a new analysis method for the LED intensity was developed [P3]. The method provides information about the size and location of the LED virtual source and directivity

of the LED. The luminous intensity values of various LEDs were analyzed with the new method.

5.1 PRINCIPLE OF THE ANALYSIS METHOD

Measuring irradiance/illuminance produced by an LED is analogous to the case where a lens (LED package/single lens) is situated between two apertures of which one corresponds to the LED chip source and the other to the radiometer/photometer entrance aperture. The optical system may be transformed to an equivalent optical system of two apertures by replacing the LED source by its virtual image having different size and location. Briefly, this is accomplished by determining irradiance/illuminance values at various distances d in the far field and by measuring the angular intensity distribution of the LED under study. The LED angular intensity distribution is fitted to $\cos^n \theta$ function by varying the value of n to evaluate the LED directivity. Finally, those irradiance/illuminance values $E_{e\nu}$ are fitted to equation (19) where D is now decomposed as the sum of d and offset Δd . [P3]

The data fit is made by minimizing the relative standard deviation of the luminous intensity values at varying distances using the offset Δd and the radius r_0' of the virtual image of the LED source as free parameters. As a result of the procedure, the radiant/luminous intensity, the size and the location of the virtual LED image source are obtained. [P3]

5.2 RESULTS OF THE LUMINOUS INTENSITY ANALYSES OF LEDs

The procedure for analyzing the LED luminous intensity was tested on 17 LEDs. The values of the directivity parameter n of the LEDs were determined from the angular distribution measurements at 0.3 m distance. The directivity of the studied LEDs varied quite a lot from $n = 0.4$ to 1915. In most cases, n was smaller than 100 [P3]. Figure 16 presents the angular distribution fit of a 5-mm yellow LED to $\cos^n \theta$ function. The angular distributions of a few LEDs were also measured at different distances to investigate if the beam width of the radiation pattern remains unchanged. Results presented in [P3] indicated that, beyond the 0.2 m distance, the beam width in the cases of each tested LED did not narrow anymore. Therefore it was reasonable to make

illuminance measurements in the distance range 0.2 – 0.8 m. The measurements were performed with 0.1 m steps to get sufficient data for fitting.

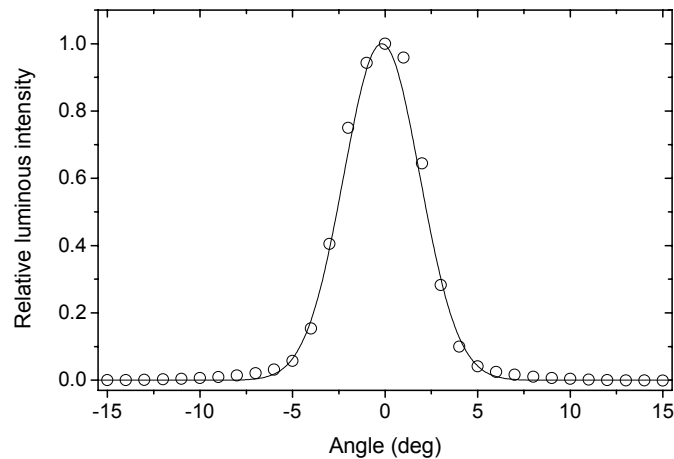


Figure 16. Fit of the angular distribution of a 5 mm yellow LED to $\cos^n \theta$. The value of n was 810.

The modified inverse-square law method produced much more consistent results for the luminous intensity values of different types of LEDs than any other method studied so far [P3]. Using the new method, the illuminance produced by an LED may be modeled accurately over a broad distance range as the LED luminous intensity remains unchanged. As a spin-off result, quite good estimates for the dimensions of the LED virtual source are also achieved. This can be utilized, e.g., in determining the LED luminance/radiance.

Results of the luminous intensity analysis also showed that LEDs had in most cases relatively large image sources and the effective source locations deviated quite a lot from the physical locations [P3]. In some cases, LEDs could be considered as point sources. This is understandable especially for LEDs without lenses. In addition, the results suggest possibility of the point source analysis for some LEDs with lenses. One reason for that might be the measurements on the mechanical axis of the LEDs because the size of the image source and the luminous intensity value were larger on the optical axis than on the mechanical axis. Figure 17 shows the variation of the visual size of the source as viewed in different directions. In the method, the LED source was modeled by a circular source. In practice, the LED chips producing light are mostly square shaped and thus their image source is obviously somewhat rectangular (Figure 17). However, the circular source approximation gives a good estimate for the image source

which is hard to determine precisely. The size of the LED virtual image source obtained with the modified inverse-square law method was in some cases larger than the physical dimensions of the LED package.



Figure 17. Photograph of the virtual source of an orange 10-mm LED taken in different directions. The third photograph from the left shows the image source on the optical axis.

The measurement results also suggest that the illuminance measurements should be performed along the optical symmetry axis of the LED. In most cases, the maximum intensity of the LED is on its optical axis and the LED angular distribution is symmetrical there. Thus the estimation of the LED directivity is more valid on the optical axis. Also, the repeatability of the results was much better on the optical axis than on the mechanical symmetry axis of the LED. [P3]

5.3 SIMPLIFICATION OF THE METHOD

The analysis method presented above needs quite a lot of experimental efforts and the computational effort is not insignificant either. Therefore, it is of interest to investigate whether it is possible to simplify the method somehow without losing the accuracy. Illuminance measurements cannot be got rid of but the angular distribution measurements might be omitted. In [P3,P4], an approximation where the accuracy requirements had been loosened, was compared to the complete method. In the approximation, the angular distribution measurements of LEDs were bypassed and an assumption of a Lambertian source for the LED intensity analysis was made. The data fit was done as earlier in section 5.1.

The luminous intensity obtained was quite consistent with that analyzed by the complete method when the width of the LED intensity distribution was more than 10° (see Figure 18). This parameter is usually specified in LED datasheets. Therefore the user can evaluate the need for angular distribution measurements and analyses of the LED in question. The use of equation (22) causes losing information about the

dimensions of the LED virtual source. Equation (22) cannot be used for evaluating the radiance/luminance, because fitting parameter r_0' becomes larger especially in the case of highly directional LEDs therefore r_0' consists of the value of n . Instead, equation (22) may be applied to analyzing the distance dependence of the LED illuminance.

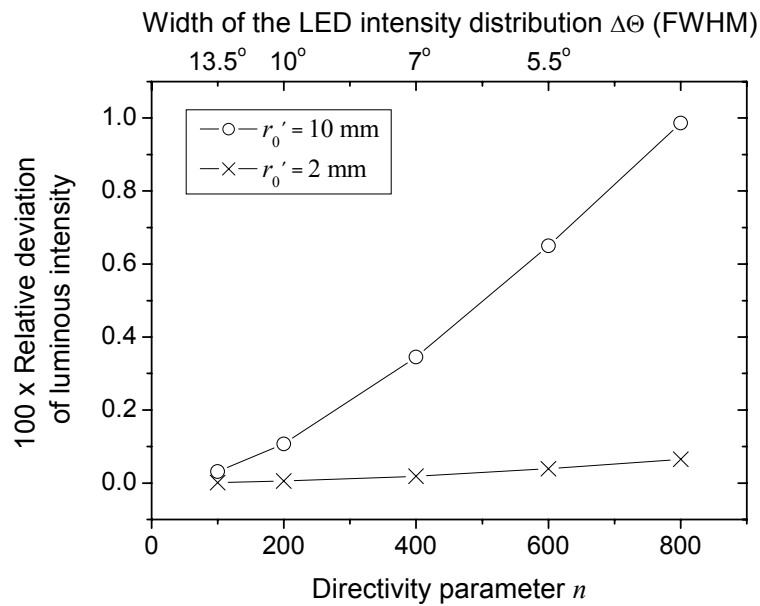


Figure 18. Relative deviation of the luminous intensity obtained with two analysis methods. (see [P4] for details)

5.4 APPLICATIONS

The analysis method developed can be utilized to design LED-array-based luminaires more efficiently. In many applications, e.g. in medical lighting, where uniform irradiance conditions are needed, the LED spacing [94] in the LED array could be analyzed more properly by taking into account the size and location of the apparent LED source in modeling the irradiance/illuminance of the LED array.

Another potential application of the method is the measurement of the radiance/luminance of LEDs. CIE technical committee TC 2-58 was established to prepare a technical report with recommendations for measurement of LED radiance and luminance, with particular attention for evaluating the photobiological safety [95, 96]. In the assessment of photobiological safety, the size of the apparent LED source is

a crucial parameter [97]. LED radiance/luminance describing the surface brightness might be determined with the new proposed method by calculating the ratio of the radiant/luminous intensity to the area of the virtual image source as measured with the method of section 5.1. Brightness measurements of LEDs should be made on the optical axis to maximize the obtained brightness. Otherwise, the harmfulness of LEDs would be underestimated.

The analysis method can be applied for determining the radiant intensity of UVLEDs as well [98,99]. UVLEDs are used in a wide variety of applications including, e.g., photocatalytic processes, displays, high-resolution optics, and UV-induced lighting. It is probable that similar measurement problems are encountered in the case of UV LEDs as with visible LEDs, because they consist of basically the same kind of structure in terms of their package and semiconductor chip.

6 BEHAVIOR OF LIGHT-EMITTING DIODES UNDER PULSE-WIDTH MODULATION

Pulse-width modulation (PWM) is frequently used as a dimming method of LEDs. LEDs have been supposed to be immune to temperature changes and color variations during the PWM control. Current reduction for dimming LEDs is not so popular because the intensity of LEDs, especially in the case of InGaN LEDs, has non-linear dependence on driving current. Furthermore, the spectra of visible InGaN LEDs have blueshifts with increasing currents, whereas the spectra of AlGaInP LEDs do not change with current [100]. On the other hand, the spectrum of the AlGaInP LED is a function of temperature whereas InGaN LEDs are notably insensitive to changes of temperature [100]. Also, using the PWM, an LED can be dimmed below 0.05 % of the maximum light output [101] whereas, with the LED current reduction, the LED brightness may be adjusted only down to 10 %. It is often assumed that PWM dimming of LEDs does not change the shape of the LED spectrum [38]. However, the authors in [102,103] found spectral variations for high-power LEDs when using the PWM dimming. These changes were small as compared to changes caused by current modulation. Recently in 2008, rapid variations in the temperatures of AlGaInP high power LEDs at the pulsed operation [104] and large changes in the junction temperatures of AlInGaN high power UVLEDs under PWM [105] were detected. The authors in [105] found a linear correlation between the junction temperature (T_j) and duty cycle (D). The coefficients dT_j/dD for the UVLEDs became larger with increasing currents and they were larger than those of the low-power LEDs studied in [P5], likely due to the higher electrical power.

In this section, the influence of the PWM on electroluminescence (EL) spectra of low-power LEDs is investigated. Changes in the junction and charge carrier temperatures of three AlGaInP LEDs under the PWM control are evaluated [P5]. In addition to the results of [P5], the spectral characteristics of three InGaN LEDs and the dependence of the color shift of the AlGaInP LEDs on modulation frequency are presented.

6.1 PULSE-WIDTH MODULATION SCHEME

Dimming LEDs by the PWM control is based on the use of a rectangular-shaped driving current as shown in Figure 19. In the PWM dimming, width t of the rectangular pulse is modulated as the period T of the modulation signal and driving current i_0 at the top of the pulse are constant. The effective current given by

$$i_{\text{eff}} = \frac{t}{T} i_0 = D i_0 \quad (23)$$

can be changed by varying the duty cycle D , in other words, by varying the pulse width t . As a result of the modulation, effective brightness B_{eff} of the LED under the PWM control obeys the corresponding equation as i_0 is substituted by B_0 , which is the LED brightness obtained at the continuous current i_0 . As a modulation frequency, $f = 1/T$, 180 Hz is often used in LED displays. In some LED applications, frequencies above audible frequency range have been recommended to be used. However, very high frequencies in the PWM scheme require design of a more expensive device. [101]

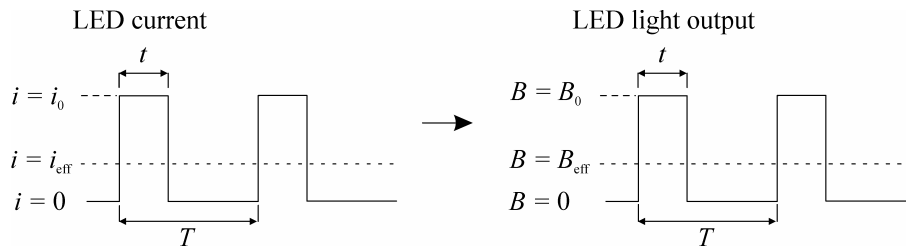


Figure 19. Illustration of the LED dimming with the PWM control. The effective current (brightness) is obtained by multiplying the current (brightness) at the continuous mode by the duty cycle $D = t/T$.

6.2 EXPERIMENTAL SET-UP

The experimental setup consisted of a spectroradiometer, an LED temperature controller with control electronics, and a pulsed current source. The LEDs studied were six epoxy-encapsulated, low-power commercial LEDs. The blue, cyan and green LEDs were made of $\text{In}_x\text{Ga}_{1-x}\text{N}$ -based material whereas the others were AlGaInP -based yellow, orange and red LEDs. To characterize the temperatures of the LEDs, the temperature of the LED under study was controlled with an aluminum body equipped

with a Peltier element and an NTC thermistor. With the pulse current source, the width t of the current pulse and the modulation frequency $f = 1/T$ could be changed. The emission spectra of the LEDs were recorded with a calibrated Minolta CS1000 spectroradiometer working in radiance mode. The recorded spectra were averaged over several pulses [P5].

6.3 RESULTS AND DISCUSSIONS

6.3.1 Spectral power distributions

The spectral behaviors of the LEDs under the PWM control were studied by measuring the EL spectra of LEDs at different duty cycles. The duty cycles of the LEDs were varied between 3 % and 100 %. The drive current of the LEDs was 20 mA and the modulation frequency f was 1 kHz. The spectral measurements were carried out after stabilizing the temperature and light output of the LED under test. The stabilization took a couple of minutes depending on the magnitude of the duty-cycle change.

The results are presented in Figure 20. The EL spectra of the InGaN LEDs do not change much under PWM dimming, but for the AlGaInP LEDs, the variations are significantly larger. With the PWM dimming, the peak wavelengths shift towards shorter wavelengths and the bandwidths become narrower. A linear relationship between the peak wavelength and bandwidth of the AlGaInP LEDs and their duty cycle was found [P5]. The peak wavelengths of the AlGaInP LEDs shift notably more than those of the InGaN LEDs, whereas the bandwidths of the InGaN LEDs become a little bit narrower than those of the AlGaInP LEDs. The largest peak wavelength shift and bandwidth narrowing within the studied duty-cycle range were 2.3 nm for the yellow LED and 1.2 nm for the blue LED.

The blueshift of the peak wavelength with decreasing duty cycle can be explained by cooling of the semiconductor chip, because the band gap energy becomes broader as the temperature drops, whilst the bandwidth narrowing is a result of the changes in the charge carrier temperature [P5,106]. The temperature effect during the PWM dimming can be understood with alternate heating and cooling of the LED chip when the current pulse is at high and low phases, respectively. With decreasing duty cycle,

the relation of the heating rate to the cooling rate decreases. As a result, the LED spectrum moves toward the shorter wavelengths.

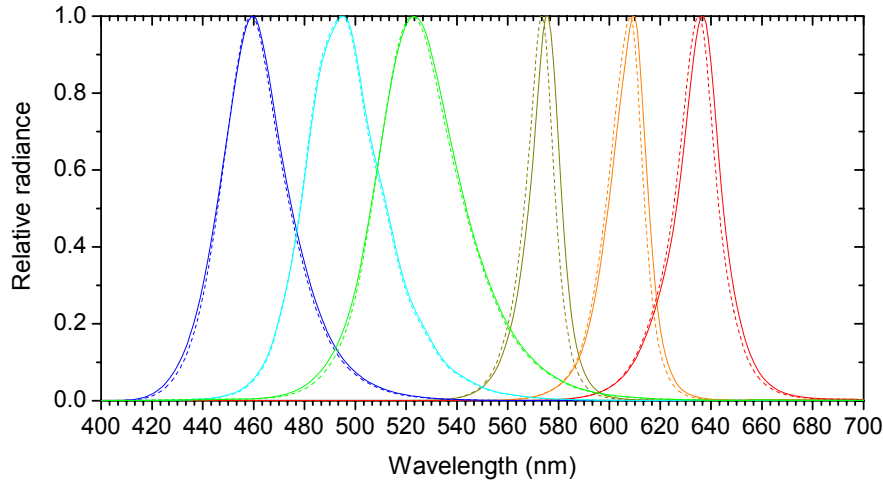


Figure 20. EL spectra of LEDs with different colors at duty cycles of 3 % (dashed lines) and 90 % (solid lines).

6.3.2 Junction temperatures

To find out the junction temperature of LEDs under the PWM control, yellow, orange, and red AlGaInP LEDs were calibrated for the peak-wavelength shift with junction temperature [P5,107-110]. The studied LEDs were connected to thermal contact with the aluminum body, whose temperature was adjusted within 15-45 °C. As the duty cycle of the LED in the junction temperature calibration measurement was low, approximately 0.3 %, LED's self-heating was considerably low. Then the temperature of the aluminum body, which was measured with a thermistor, could be assumed to equal to that of the LED. The peak wavelengths were determined from the EL spectra of the LEDs at different temperatures [P5]. By knowing the temperature and peak wavelength of the LED, junction temperature coefficient $d\lambda_p/dT_j$ of the peak wavelength for three AlGaInP LEDs was determined [P5]. The junction temperature of the LED at the known duty cycle may be inferred from the peak-wavelength positions determined earlier. Then duty cycle coefficient dT_j/dD of the junction temperature for the AlGaInP LEDs could be determined.

Figure 21 shows the results from the determination of the junction temperature of the LEDs during the PWM control. Coefficient $d\lambda_p/dT_j = 0.1384 \text{ nm}/^\circ\text{C}$ for the red AlGaInP

LED shows good agreement with the values of 0.1562, 0.1157, and 0.1376 nm/°C published elsewhere [107-109]. The change in the junction temperature of the LEDs is even more than 20 °C. That change is so large that the temperatures of the LEDs at different duty cycles should be appended in the LED datasheets.

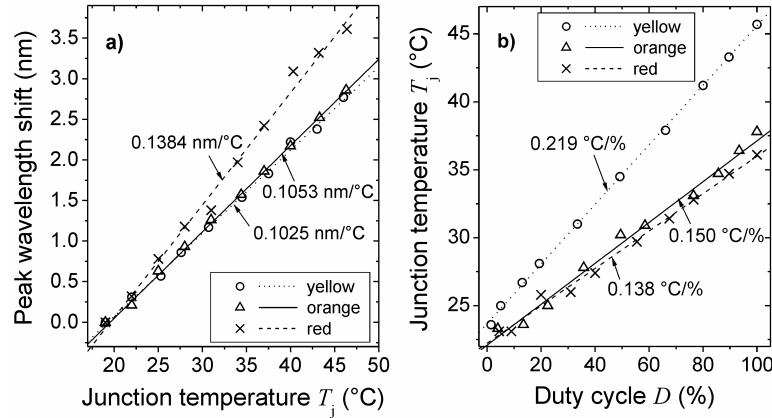


Figure 21. a) The peak wavelength shifts with the junction temperature and b) the junction temperatures at different duty cycles for the studied AlGaInP LEDs. Junction temperature coefficient $d\lambda_p/dT_j$ of the peak wavelength and duty cycle coefficient dT_j/dD of the junction temperature for each LED is shown. [P5]

6.3.3 Color coordinates

To investigate whether the changes in the EL spectra of the LEDs cause color variations, which could be perceived by a human eye, color coordinates of the studied LEDs were calculated in the CIE 1976 ($u'v'$) chromaticity diagram using the color matching functions of the CIE 1931 2° standard colorimetric observer. The color coordinates for the LEDs are shown in Figure 22. The changes in the spectra of the InGaN LEDs and the red AlGaInP LED under the PWM dimming do not cause perceivable color variations. However, the changes in the chromaticity coordinates of the yellow and orange LEDs are significant because the chromaticity changes of 0.003 in that wavelength region of the CIE 1976 chromaticity diagram may be perceived by the human eye. [P5,106]

In addition, dependence of the colorimetric characteristics of the orange and yellow LEDs on modulation frequency was studied. The duty cycle was varied from 100 % to 3 % by a few steps for modulation frequencies f of 180, 500 and 1000 Hz. The color shift $\Delta u'v'$ in the PWM dimming made at these modulation frequencies were calculated. The

values of modulation frequency coefficient $d(\Delta u'v')/df$ of the color shift determined for the orange and yellow LEDs were 0.0006 1/kHz and 0.002 1/kHz, respectively (see Figure 23). This implies that the color shift becomes larger at high modulation frequencies and the use of tens of kHz may cause notably more significant color shifts, as Figure 22 indicates. Thus, the results obtained herein suggest that, in PWM drivers of LEDs, as slow modulation as possible should be used. The flickering effect produces the lower limit for a reasonable modulation frequency.

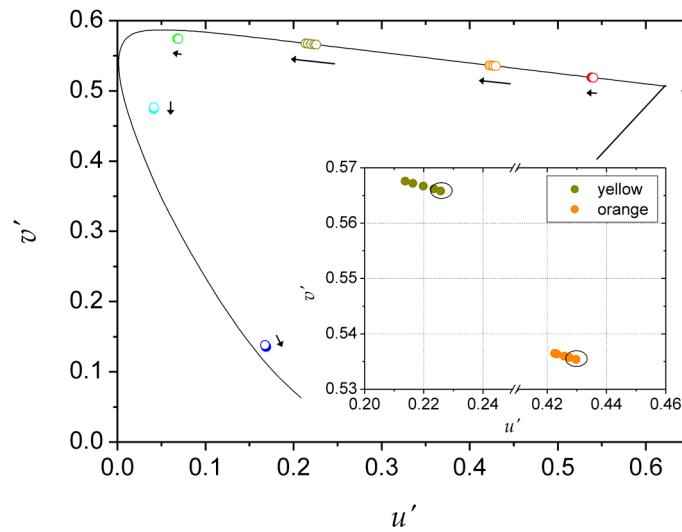


Figure 22. $u'v'$ -coordinates of the LEDs at different duty cycles. The arrows show the direction and the magnitude of the color change as the duty cycle decreases. The circles indicate approximately MacAdam ellipses [P5,106].

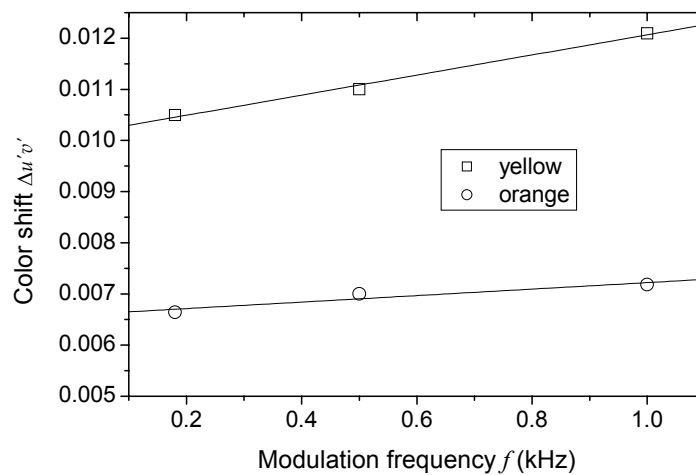


Figure 23. Modulation frequency dependence of the color shift for two LEDs.

7 CONCLUSIONS

In this thesis, a new effect in the measuring heads of solar UV spectroradiometers has been presented. The reference plane distance offset of a diffuser in a spectroradiometer calibration may cause measurement errors of more than 2 % for solar UV irradiance. This means, e.g., that a spectroradiometer equipped with one of the most popular diffusers for solar UV monitoring in Europe overestimates solar irradiance radiation systematically by a couple of percents. Earlier solar UV data may be corrected using a simple correction factor, if the spectroradiometer diffuser has been calibrated for the reference plane position. Also, it was noted that the measured offsets correlate with the cosine errors of the angular responsivities of the diffusers. Thus, the known angular responsivity curves can be used to predict whether the distance offsets of the diffusers need to be measured.

A novel method for determining radiant/luminous intensities of LEDs was presented. The model takes into account the size and location of the virtual LED source. The method was tested for luminous intensities of 17 LEDs with different colors, packages, angular distributions, and power levels. The new method gave significantly more consistent results for the LED luminous intensities at a large distance range than any other method presented so far. Illuminance measurements are recommended to be made at quite large distances from the LED due to the distance dependence of the LED angular distribution in the near field. Also, the optical axis should be used as the measurement axis, because the results obtained on the optical axis are more reproducible than those obtained on the mechanical axis.

The spectral, thermal, and colorimetric behaviors of six LEDs in the PWM dimming were studied. Changes in the EL spectra of the LEDs were observed. Blueshift of the peak wavelength with decreasing duty cycle was found for both InGaN and AlGaInP LEDs. The spectrally changing feature was demonstrated to be the result of the temperature change in the LED. The changes in the temperatures of the studied LEDs under the PWM control varied from 13 °C to 22 °C depending on the emission

wavelength of the LED. The chromaticity coordinates of the yellow and orange LEDs in the $u'v'$ diagram varied as much as 0.012 and 0.007 within the studied duty-cycle range, respectively. These color shifts may be perceived by the human eye. Thus, it might be useful to include information about spectral, thermal, and color variations under PWM control in the datasheets of the LED manufacturers.

REFERENCES

1. J. Gröbner, M. Blumthaler, S. Kazadzis, A. Bais, A. Webb, J. Schreder, G. Seckmeyer, and D. Rembges, *Metrologia* **43**, S66–S71 (2006).
2. K. Garane, A. F. Bais, S. Kazadzis, A. Kazantzidis, and C. Meleti, *Ann. Geophys.* **24**, 3215–3228 (2006).
3. M. Blumthaler, *Radiat. Prot. Dosimetry* **111**, 359–362 (2004).
4. J. Metzdorf, K. D. Stock, P. Sperfeld, A. Sperling, S. Winter, and T. Wittchen, *Metrologia* **40**, S66–S69 (2003).
5. R. R. Cordero, G. Seckmeyer, D. Pissulla, L. DaSilva, and F. Labbe, *Meas. Sci. Technol.* **19**, 045104 (2008).
6. G. Bernhard and G. Seckmeyer, *J. Geophys. Res.* **104**, 14321–14345 (1999).
7. G. Bernhard, R. L. McKenzie, M. Kotkamp, S. Wood, C. R. Booth, J. C. Ebrahimian, P. Johnston, and S. E. Nichol, *J. Geophys. Res.* **113**, D14310 (2008).
8. J. A. Martinez-Lozano, M. P. Utrillas, R. Pedrós, F. Tena, J. P. Diaz, F. J. Expósito, J. Lorente, X. de Cabo, V. Cachorro, R. Vergaz, and V. Carreño, *J. Atmos. Ocean. Technol.* **20**, 997–1010 (2003).
9. J. Gröbner, J. Schreder, S. Kazadzis, A. F. Bais, M. Blumthaler, P. Görts, R. Tax, T. Koskela, G. Seckmeyer, A. R. Webb, and D. Rembges, *Appl. Opt.* **44**, 5321–5331 (2005).
10. J. Gröbner, *Appl. Opt.* **42**, 3516–3521 (2003).
11. J. G. Schreder, M. Blumthaler, and M. Huber, *Internet Photochem. Photobiol.* <http://www.photobiology.com/UVR98/schreder/index.htm>
12. G. Bernhard and G. Seckmeyer, *Photochem. Photobiol.* **65**, 923–930 (1997).
13. E. A. Early, E. A. Thompson, and P. Disterhoft, *Appl. Opt.* **37**, 6664–6670 (1998).
14. A. F. Bais, S. Kazadzis, K. Garane, N. Kouremeti, J. Gröbner, M. Blumthaler, G. Seckmeyer, A. R. Webb, T. Koskela, P. Görts, and J. Schreder, *Appl. Opt.* **44**, 7136–7143 (2005).
15. P. Kärhä, L. Ylianttila, T. Koskela, K. Jokela and E. Ikonen, *Metrologia* **40**, S17–S20 (2003).
16. S. D. Pye and C. J. Martin, *Phys. Med. Biol.* **45**, 2701–2712 (2000).

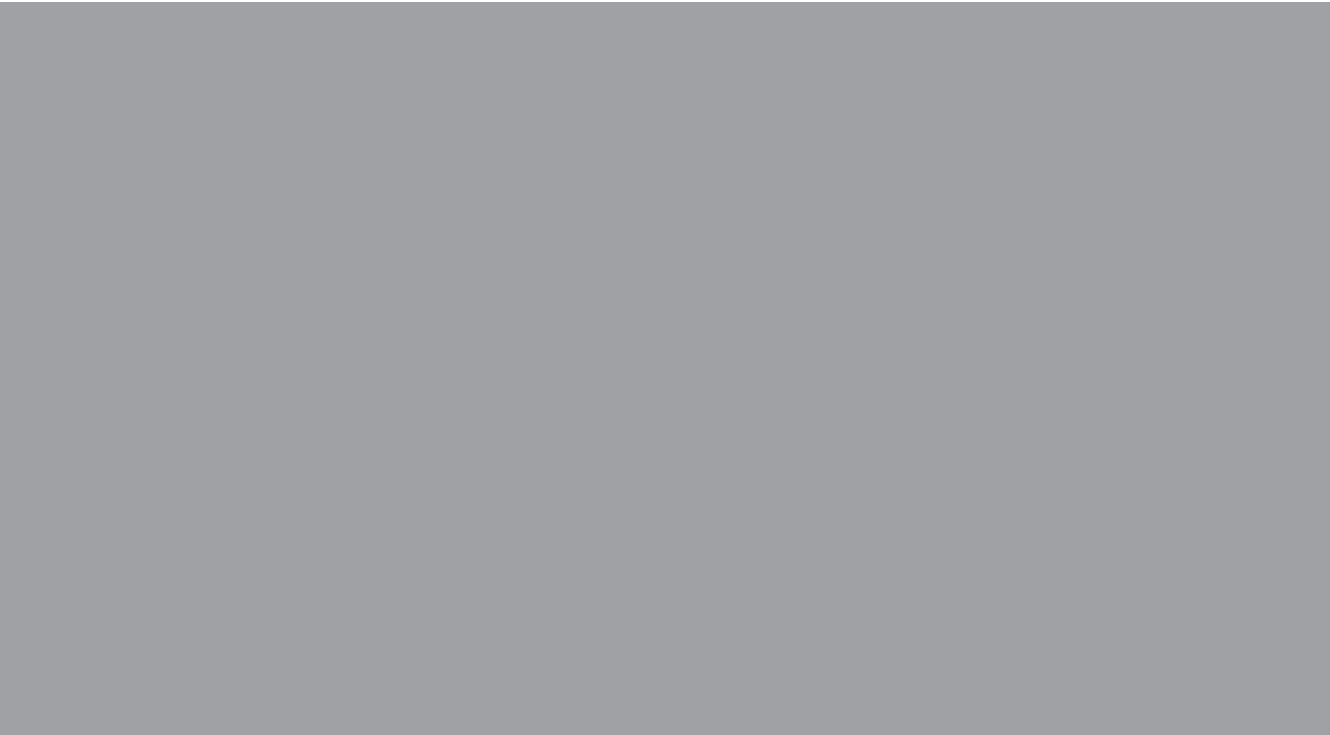
17. L. P. Boivin, *Appl. Opt.* **21**, 918-923 (1982).
18. R. D. Saunders and H. J. Kostkowski, *Appl. Opt.* **28**, 3242–3245 (1989).
19. L. Ylianttila and J. Schreder, *Opt. Mat.* **27**, 1811-1814 (2005).
20. B. G. Gardiner, “Spectroradiometer calibration methods and techniques,” in *Solar Ultraviolet Radiation*, eds. C. S. Zerefos, A. F. Bais (Springer, Tessaaloniki, Greece, 1997) 121–122.
21. J. Hovila, M. Mustonen, P. Kärhä, and E. Ikonen, *Appl. Opt.* **44**, 5894–5898 (2005).
22. Measurement of LEDs, CIE127.2 (Revision of CIE127-1997), TC-45, Draft no. 4, (2004).
23. N. Holonyak and S. F. Bevacqua, *Appl. Phys. Lett.* **1**, 82–83 (1962).
24. R. A. Logan, H. G. White, and W. Wiegmann, *Solid State Electron* **14**, 55–70 (1971).
25. M. G. Craford, D. L. Keune, W. O. Groves, and A. H. Herzog, *J. Elec. Mat.* **2**, 137–158 (1973).
26. S. Nakamura, T. Mukai, and M. Senoh, *Appl. Phys. Lett.* **64**, 1687–1689 (1994).
27. C. P. Kuo, R. M. Fletcher, T. D. Osentowski, M. C. Lardizabal, M. G. Craford, and V. M. Robbins, *Appl. Phys. Lett.* **57**, 2937–2939 (1990).
28. E. F. Schubert and J. K. Kim, *Science* **308**, 1274–1278 (2005).
29. M. R. Krames, O. B. Shchekin, R. Mueller-Mach, G. O. Mueller, L. Zhou, G. Harbers, and M. G. Craford, *J. Disp. Technol.* **3**, 160–175 (2007).
30. D. A. Steigerwald, J. C. Bhat, D. Collins, R. M. Fletcher, M. O. Holcomb, M. J. Ludowise, P. S. Martin, and S. L. Rudaz, *IEEE J. Selected Topics Quantum Electron.* **8**, 310–320 (2002).
31. S. Nakamura, *Proc. SPIE* **3002**, 26–35 (1997).
32. J. Han, M. H. Crawford, R. J. Shul, J. J. Figiel, M. Banas, L. Zhang, Y. K. Song, H. Zhou, and A. V. Nurmikko, *Appl. Phys. Lett.* **73**, 1688–1690 (1998).
33. R. Mueller-Mach, G. O. Mueller, M. R. Krames, and T. Trottier, *IEEE J. Selected Topics Quantum Electron.* **8**, 339–345 (2002).
34. R. Mueller-Mach, G. Mueller, M. R. Krames, H. A. Höpfe, F. Stadler, W. Schnick, T. Juestel, and P. Schmidt, *phys. stat. sol. (a)* **202**, 1727–1732 (2005).
35. R.-J. Xie, N. Hirosaki, K. Sakuma, Y. Yamamoto and M. Mitomo, *Appl. Phys. Lett.* **84**, 5404–5406 (2004).
36. J. K. Park K. J. Choi, J. H. Yeon, S. J. Lee, and C. H. Kim, *Appl. Phys. Lett.* **88**, 043511 (2006).

37. T. Kim and S. Kang, *J. Lumin.* **122-123**, 964–966 (2007).
38. S. Muthu, F. J. P. Schuurmans, and M. D. Pashley, *IEEE J. Selected Topics Quantum Electron.* **8**, 333–338 (2002).
39. M. Yamada, Y. Narukawa, and T. Mukai, *Jpn. J. Appl. Phys.* **41**, L246–L248 (2002).
40. J. Y. Tsao, *IEEE Circuits & Devices Magazine*, May/June 2004.
41. S. W. Brown, C. Santana, and G. P. Eppeldauer, *J. Res. Natl. Inst. Stand. Technol.* **107**, 363–371 (2002).
42. I. Fryc, S. W. Brown, G. P. Eppeldauer, and Y. Ohno, *Opt. Eng.* **44**, 111309 (2005).
43. S. W. Brown, J. P. Rice, J. E. Neira, B. C. Johnson, and J. D. Jackson, *J. Res. Natl. Inst. Stand. Technol.* **111**, 401–410 (2006).
44. C. C. Miller, Y. Zong, and Y. Ohno, *Proc. SPIE* **5530**, 69–79 (2004).
45. Y. Ohno, *Proc. SPIE* **6046**, 604625 (2006).
46. C. C. Miller and Y. Ohno, Proc. CIE Expert Symposium, May 11–12, 2001, Gaithersburg, Maryland, USA (2001).
47. J. M. Benavides and R. H. Webb, *Appl. Opt.* **44**, 4000–4003 (2005).
48. D. R. Agaphonov, V. S. Ivanov, V. I. Sapritsky and R. I. Stolyarevskaya *Metrologia* **37**, 587–590 (2000).
49. S. Park, D.-H. Lee, Y.-W. Kim, and S.-N. Park, *Appl. Opt.* **46**, 2851–2858 (2007).
50. J. Hovila, P. Kärha, L. Mansner, and E. Ikonen, *Opt. Eng.* **43**, 170–173 (2004).
51. K. Godo, T. Saito, H. Shitomi, T. Zama, and I. Saito, *Proc. NEWRAD2005*, 199 (2005).
52. G. Sauter, *Metrologia* **28**, 239–242 (1991).
53. M. Bürmen, F. Pernuš, and B. Likar, *Meas. Sci. Technol.* **17**, 1372–1378 (2007).
54. G. T. Gillies, *Am. J. Phys.* **48**, 418–419 (1980).
55. K. Muray, *Appl. Opt.* **30**, 2178–2186 (1991).
56. A. W. Norris, M. Bahadur, and M. Yoshitake, *Proc. SPIE* **5941**, 1-7 (2005).
57. I. Moreno and C.-C. Sun, *Opt. Express* **16**, 1808–1819 (2008).
58. L. Mandel and E. Wolf, *Coherence and Quantum Optics*, (Cambridge University Press, 1995, chapter 5).
59. P. Vahimaa and J. Turunen, *Opt. Express* **14**, 1376–1381 (2006).
60. J. Turunen and P. Vahimaa, *Opt. Express* **16**, 6433–6442 (2008).
61. T. Araki and H. Misawa, *Rev. Sci. Instrum.* **66**, 5469–5472 (1995).

62. M. Meneghini, S. Podda, A. Morelli, R. Pintus, L. Trevisanello, G. Meneghesso, M. Vanzi, and E. Zanoni, *Microelectron. Rel.* **46**, 1720–1724 (2006).
63. D. I. Lawson and D. Hird, *Brit. J. Appl. Phys.* **5**, 72–74 (1954).
64. J. W. T. Walsh, *Photometry*, Dover, New York, 1965.
65. D. S. Goodman, *Appl. Opt.* **24**, 3240–3248 (1985).
66. S. Tryka, *J. Mod. Opt.* **53**, 365–380 (2006).
67. L. Fu, R. Leutz, and H. Ries, *J. Appl. Phys.* **100**, 103528 (2006).
68. L. Fu, R. Leutz, and H. Ries, *Proc. SPIE* **6338**, 633802 (2006).
69. R. F. Rykowski and C. B. Wooley, *Proc. SPIE* **3130**, 204–208 (1997).
70. R. L. Farrow, R. Trebino, and R. E. Palmer, *Appl. Opt.* **26**, 331–335 (1987).
71. L. P. Boivin, A. A. Gaertner, and D. S. Gignac, *Metrologia* **24**, 139–152 (1987).
72. E. Ikonen, P. Kärhä, A. Lassila, F. Manoochehri, H. Fagerlund, and L. Liedquist, *Metrologia* **32**, 689–692 (1995/96).
73. W. Erb and G. Sauter, *Metrologia* **34**, 115–124 (1997).
74. T. M. Goodman and P. J. Key, *Metrologia* **25**, 29–40 (1988).
75. C. L. Cromer, G. Eppeldauer, J. E. Hardis, T. C. Larason, Y. Ohno, A. C. Parr, *J. Res. Natl. Inst. Stand. Technol.* **101**, 109–132 (1996).
76. J. Campos, A. Corrons, A. Pons, and P. Corredera, *Metrologia* **32**, 675–679 (1995/96).
77. V. I. Sapritsky, *Metrologia* **24**, 53–59 (1987).
78. Y. Ohno, “Photometric standards,” in *Handbook of applied photometry*, C. DeCusatis, eds. (Optical Society of America, Washington DC, 1997), 55–90.
79. H. J. Kostkowski, *Reliable Spectroradiometry*, (Spectroradiometry Consulting, La Plata, MD, 1997).
80. A. F. Bais, S. Kazadzis, D. Balis, C. S. Zerefos, and M. Blumthaler, *Appl. Opt.* **37**, 6339–6344 (1998).
81. G. Seckmeyer and G. Bernhard, *Proc. SPIE* **2049**, 140–151 (1993).
82. U. Feister, R. Grewe, and K. Gericke, *Solar Energy* **60**, 313–332 (1997).
83. A. de La Casiniere, T. Cabot, and S. Benmansour, *Solar Energy* **54**, 173–182 (1995).
84. J. Gröbner, M. Blumthaler, and W. Ambach, *Geophys. Res. Lett.* **23**, 2493–2496 (1996).

85. K. Lakkala, A. Arola, A. Heikkilä, J. Kaurola, T. Koskela, E. Kyrö, A. Lindfors, O. Meinander, A. Tanskanen, J. Gröbner, and G. Hülsen, *Atmos. Chem. Phys.* **8**, 3369–3383 (2008).
86. G. Xu and X. Huang, *Metrologia* **37**, 235–242 (2000).
87. G. Xu, X. Huang, and Y. Liu, *Metrologia* **37**, 559–562 (2000).
88. J. Gröbner and M. Blumthaler, *Opt. Lett.* **32**, 80–82 (2007).
89. H. Luo, J. K. Kim, E. F. Schubert, J. Cho, C. Sone, and Y. Park, *Appl. Phys. Lett.* **86**, 243505 (2005).
90. T. V. Cuong, H. S. Cheong, and C.-H. Hong, *phys. stat. sol. (c)* **1**, 2433–2437 (2004).
91. M. R. Krames, M. Ochiai-Holcomb, G. E. Höfler, C. Carter-Coman, E. I. Chen, I.-H. Tan, P. Grillo, N. F. Gardner, H. C. Chui, J.-W. Huang, S. A. Stockman, F. A. Kish, M. G. Craford, T. S. Tan, C. P. Kocot, M. Hueschen, J. Posselt, B. Loh, G. Sasser, and D. Collins, *Appl. Phys. Lett.* **75**, 2365–2367 (1999).
92. K. Muray, *Proc. Soc. Photo-Opt.* **954**, 560–567 (1988).
93. P. Kärhä, P. Manninen, J. Hovila, L. Seppälä, and E. Ikonen, *Proc. NEWRAD2005*, 211–212 (2005).
94. I. Moreno, M. Avendaño-Alejo, and R. I. Tzonchev, *Appl. Opt.* **45**, 2265–2272 (2006).
95. W. Horak, *Light & Engineering* **15**, 75–79 (2007).
96. CIE Technical committee TC 2-58, Measurement of LED radiance and luminance (private communication).
97. M. Tongsheng, L. Yiqing, Y. Jiandong, and W. Jianping, *Light & Engineering* **15**, 91–93 (2007).
98. D. Morita, M. Sano, M. Yamamoto, T. Murayama, S.-I. Nagahama and T. Mukai, *Jpn. J. Appl. Phys.* **41**, L1434-L1436 (2002).
99. S.-R. Jeon, M. Gherasimova, Z. Ren, J. Su, G. Cui, J. Han, H. Peng, Y.-K. Song, A. V. Nurmikko, L. Zhou, W. Goetz, and M. Krames, *Jpn. J. Appl. Phys.* **43**, L1409-L1412 (2004).
100. T. Mukai, M. Yamada, and S. Nakamura, *Jpn. J. Appl. Phys.* **37**, L1358-L1361 (1998).
101. R. S. Simpson, *Lighting control - technology and applications*, Oxford: Focal Press, 2003.
102. M. Dyble, N. Narendran, A. Bierman, and T. Klein, *Proc. SPIE* **5941**, 291-299 (2005).
103. Y. Gu, N. Narendran, T. Dong, and H. Wu, *Proc. SPIE* **6337**, 63370J (2006).

104. L. Yang, J. Hu, and M. W. Shin, *IEEE Electron Device Lett.* **29**, 863–866 (2008).
105. J. C. Zhang, Y. H. Zhu, T. Egawa, S. Sumiya, M. Miyoshi, and M. Tanaka, *Appl. Phys. Lett.* **92**, 191917 (2008).
106. E. F. Schubert, *Light Emitting Diodes*, Cambridge University Press, Cambridge, 2006.
107. S. Chhajed, Y. Xi, Y.-L. Li, T. Gessmann, and E. F. Schubert, *J. Appl. Phys.* **97**, 054506 (2005).
108. N. C. Chen, Y. N. Wang, C. Y. Tseng, and Y. K. Yang, *Appl. Phys. Lett.* **89**, 101114 (2006).
109. E. Hong and N. Narendran, *Proc. SPIE* **5187**, 93 (2004).
110. Y. Xi, J.-Q. Xi, T. Gessmann, J. M. Shah, J. K. Kim, E. F. Schubert, A. J. Fischer, M. H. Crawford, K. H. A. Bogart, and A. A. Allerman, *Appl. Phys. Lett.* **86**, 031907 (2005).



ISBN 978-951-22-9555-5
ISBN 978-951-22-9556-2 (PDF)
ISSN 1795-2239
ISSN 1795-4584 (PDF)